cmgh
CELLULAR AND MOLECULAR GASTROENTEROLOGY AND HEPATOLOGY

ORIGINAL RESEARCH

GDF15 Ameliorates Liver Fibrosis by Metabolic Reprogramming of Macrophages to Acquire Anti-Inflammatory Properties

Xiaolei Li,[1,*] Qian Huai,[1,*] Cheng Zhu,[1,*] Xu Zhang,[1] Wentao Xu,[1] Hanren Dai,[1] and Hua Wang[1,2]

[1]Department of Oncology, the First Affiliated Hospital of Anhui Medical University, Hefei, China; and [2]Inflammation and Immune Mediated Diseases Laboratory of Anhui Province, Anhui Medical University, Hefei, China

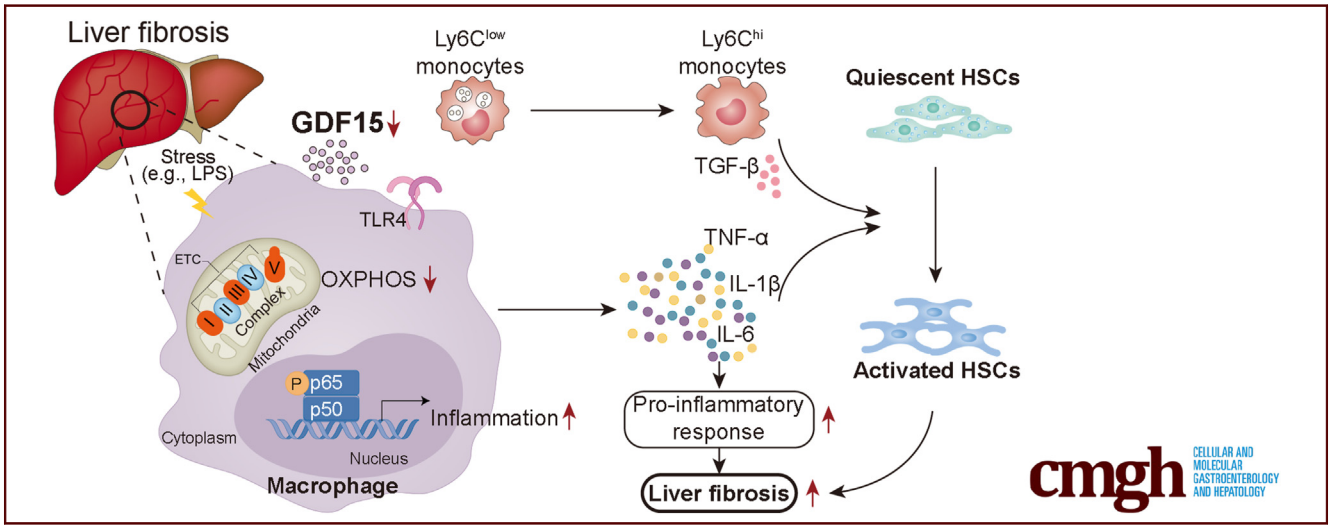

SUMMARY

Fibrosis represents the process of scarring occurring in chronic liver diseases, driven by inflammatory and immune responses, resulting in high morbidity and mortality. Herein, we found that deletion of growth differentiation factor 15 significantly exacerbated liver fibrosis and liver inflammatory response in animal models. Our data implicate the importance of growth differentiation factor 15 in macrophage programming during liver fibrosis and suggest a novel pathway that is involved in the resolution of scar tissue.

BACKGROUND & AIMS: Liver fibrosis/cirrhosis is significant health burden worldwide, resulting in liver failure or cancer and accounting for many deaths each year. The pathogenesis of liver fibrosis is very complex, which makes treatment challenging. Growth differentiation factor 15 (GDF15), a cysteine knot protein belonging to the transforming growth factor β (TGF-β) superfamily, has been shown to play a protective role after tissue injury and to promote a negative energy balance during obesity and diabetes. However, paucity of literature is available about GDF15 function in liver fibrosis. This study aimed to investigate the immunomodulatory role and therapeutic potential of GDF15 in progression of hepatic fibrosis.

METHODS: GDF15 expression was studied in patients with fibrosis/cirrhosis and in 2 murine models of liver fibrosis, including mice treated with CCl_4 or DDC diet. GDF15 involvement in the pathogenesis of liver fibrosis was assessed in *Gdf15* knockout mouse using both CCl_4 and DDC diet experimental models. We used the CCl_4 and/or DDC diet–induced liver fibrosis model to examine the antifibrotic and anti-inflammatory effects of AAV8-mediated GDF15 overexpression in hepatocytes or recombinant mouse GDF15.

RESULTS: GDF15 expression is decreased in the liver of animal models and patients with liver fibrosis/cirrhosis compared with those without liver disease. In vivo studies showed that GDF15 deficiency aggravated CCl_4 and DDC diet–induced liver fibrosis, while GDF15 overexpression mediated by AAV8 or its recombinant protein alleviated CCl_4 and/or DDC diet–induced liver fibrosis. In *Gdf15* knockout mice, the intrahepatic microenvironment that developed during fibrosis showed relatively more inflammation, as demonstrated by enhanced infiltration of monocytes and neutrophils and increased expression of proinflammatory factors, which could be diminished by AAV8-mediated GDF15 overexpression in hepatocytes. Intriguingly, GDF15 exerts its effects by reprogramming the metabolic pathways of macrophages to acquire an oxidative phosphorylation–dependent anti-inflammatory functional fate. Furthermore, adoptive transfer of GDF15-preprogrammed macrophages to mouse models of liver fibrosis induced by CCl_4 attenuated inflammation and alleviated the progression of liver fibrosis.

CONCLUSION: GDF15 ameliorates liver fibrosis via modulation of liver macrophages. Our data implicate the importance of the liver microenvironment in macrophage programming during liver fibrosis and suggest that GDF15 is a potentially attractive therapeutic target for the treatment of patients with liver fibrosis. *(Cell Mol Gastroenterol Hepatol 2023;16:711–734; https://doi.org/10.1016/j.jcmgh.2023.07.009)*

Keywords: GDF15; Liver Fibrosis; Inflammation; Macrophage; Immunometabolism; Oxidative Phosphorylation.

Liver fibrosis is caused by chronic hepatic inflammation (a protracted wound healing response) and frequently develops into cirrhosis.[1,2] The loss of healthy tissue to fibrosis is responsible for up to 45% of deaths in developed countries.[3,4] The multiple etiologies of liver fibrosis include chronic viral infection, alcohol abuse, cholestasis, autoimmune, drug/toxin, and nonalcoholic steatohepatitis (NASH).[5] However, this mechanism of precise regulation is problematic and uncontrollable, especially when liver injury persists. Irrespective of initial causes, progression to liver fibrosis and its end-stage cirrhosis requires an inflammatory component.[1] Perpetuation of the fibrotic process is a continuous wound healing response mediated by the progressive activation and proliferation of extracellular matrix–expressing myofibroblasts and interaction between innate and adaptive immune cells.[2,6] Excessive wound healing due to uncontrolled hepatocyte death upon persistent tissue insults results in pathologic fibrogenesis.[7] There is still no approved targeted treatment to reverse or at least slow down the progression of liver fibrosis. Hence, studies expanding our knowledge of the fibrotic process in chronic liver diseases are important for the development of novel therapeutic strategies that control, or even reverse, tissue fibrosis.

Hepatic macrophages consistently localize in close proximity to activated myofibroblasts in areas of scar tissue and indisputably play a key role in fibrosis.[8] In the liver, macrophages can be broadly defined as either resident Kupffer cells or monocyte-derived macrophages.[9] Kupffer cells appear essential for sensing tissue injury and initiating inflammatory responses, while infiltrating Ly6C^{+} monocyte–derived macrophages are linked to chronic inflammation and fibrogenesis.[8,10–12] In congruence with the fact that liver fibrosis is a bidirectional process, hepatic macrophages can actually exert dual functions in the context of experimental liver fibrosis by either promoting or abrogating the excessive deposition of extracellular matrix.[10,13] During the initiation of liver fibrosis, hepatic macrophages are activated and rapidly secrete proinflammatory cytokines and chemokines such as interleukin (IL)-1β, tumor necrosis factor (TNF), CCL2, and CCL5, resulting in the paracrine activation of protective or apoptotic signaling pathways of hepatocytes and the recruitment of additional immune cells that booster hepatic injury.[10] In order to accommodate for the broad spectrum of macrophage function and phenotypes, these cells have been classified as either classical macrophages (M1) that can be induced by interferon γ (IFN-γ) and lipopolysaccharide (LPS) or alternatively activated macrophages (M2) that are controlled by IL-4 and IL-13, which could result in typical cytokine response profiles.[14] However, this model is by far too simplistic to describe the polarization of liver macrophages, especially in a disease context. It should be noted that in living organisms, it is very difficult to assign tissue macrophages to classical or alternative activation. In the injured liver, macrophages often express markers of inflammation or resolution simultaneously,[15,16] which can rapidly change their phenotype depending on the hepatic microenvironment.[17,18] Recent advances in immunometabolism have revealed that M1 and M2 macrophages opt for distinct metabolic pathways upon activation to meet their demands for energy and the production of specific functional-cell-associated factors.[19–21] M1 macrophages rely mainly on aerobic glycolysis, whereas M2 macrophages depend more on oxidative phosphorylation (OXPHOS).[21] Moreover, infiltrating monocytes/macrophages are critical for the initial inflammatory phase of wound healing process as in liver fibrosis. Hepatic macrophages comprise at least 2 subsets: Ly6C^{hi} and Ly6C^{low}.[15,16] Upon phenotypic analysis, the Ly6C^{hi} monocytes show an inflammatory, tissue-damaging effect during fibrogenesis, whereas the Ly6C^{low} monocytes show anti-inflammatory, tissue-protective features after end of the injury.[16] Thus, a deeper understanding of the underlying mechanisms involved in monocyte/macrophage-orchestrated chronic liver inflammation can provide valuable information that may help to halt and effectively reverse ongoing liver fibrosis.

Growth differentiation factor 15 (GDF15), originally called NSAID-activated gene 1 and macrophage inhibitory cytokine 1, is a cell stress-responsive TGF-β superfamily member historically associated with cancer cachexia, cardiovascular disease, and a host of other diseases with inflammatory etiologies.[22–24] GDF15 also has been shown to play a protective role after tissue injury and to promote a negative energy balance during obesity and diabetes.[25,26] In addition to its metabolic effects, GDF15 also regulates the

***Authors share co-first authorship.**

Abbreviations used in this paper: **α-SMA, α-smooth muscle actin; ALT, alanine aminotransferase; AST, aspartate aminotransferase; BMDM, bone marrow–derived macrophage; CM, conditional media; DMEM, Dulbecco's modified Eagle's medium; ECAR, extracellular acidification rate; ELISA, enzyme-linked immunosorbent assay; FBS, fetal bovine serum; GDF15, growth differentiation factor 15; GEO, Gene Expression Omnibus; H&E, hematoxylin and eosin; HCC, hepatocellular carcinoma; HSC, hepatic stellate cell; IFN-γ, interferon γ; IL, interleukin; KO, knockout; LPS, lipopolysaccharide; mRNA, messenger RNA; NASH, nonalcoholic steatohepatitis; NF-κB, nuclear factor κB; OXPHOS, oxidative phosphorylation; OCR, oxygen consumption rate; qRT-PCR, quantitative reverse-transcription polymerase chain reaction; rmGDF15, recombinant murine growth differentiation factor 15; TGF-β, transforming growth factor β; TNF, tumor necrosis factor; TUNEL, terminal deoxynucleotidyl transferase–mediated deoxyuridine triphosphate nick-end labeling; WT, wild-type.**

Most current article

2352-345X
https://doi.org/10.1016/j.jcmgh.2023.07.009

host's immune responses to infectious and noninfectious diseases.[24,27] However, the expression and role of GDF15 in inflammatory diseases has not been clarified, and its immunomodulatory function remains controversial. Findings in both mice and humans have shown that metformin and exercise increase circulating levels of GDF15.[28–30] GDF15 deficiency aggravated cardiac and renal injury during sepsis because of increased expression of inflammatory cytokines.[31] Thus, GDF15 might also exert anti-inflammatory effects through mechanisms that are not fully understood. These unique and distinct mechanisms for suppressing food intake and inflammation make GDF15 an appealing candidate to treat many metabolic diseases.[32] While GDF15 is induced by physiological stress, disease, or other noxious stimuli, GDF15 expression in the epidermis of psoriasis patients was decreased in association with increasing inflammation severity.[33] However, studies investigating the role of GDF15 in liver homeostasis are limited, and whether GDF15 can regulate liver fibrosis or not is largely unknown.

In the present study, we aimed to elucidate the roles and mechanisms of GDF15 during liver fibrosis. The results showed that GDF15 is significantly decreased in fibrotic livers, also negatively correlating with hepatic inflammation and fibrosis in both patient specimens and animal models. Genetic deletion of GDF15 aggravated the progression of liver fibrosis and enhanced the number of Ly6C^{hi} macrophages in mouse fibrotic liver tissues, while fibrogenesis was reduced by AAV8-mediated GDF15 overexpression in hepatocytes. Additionally, we revealed that GDF15 could shape the anti-inflammatory inclination of macrophages through setting metabolic commitment for OXPHOS. Ultimately, in an in vivo model of liver fibrosis, the transplantation of GDF15-preprogrammed macrophages contributed to control of liver injury and fibrosis. Taken together, these findings underscore novel functions of GDF15 in ameliorating the pathogenesis of liver fibrosis and represent its therapeutic potential for liver fibrosis.

Results

GDF15 Expression Is Downregulated in Human and Murine Liver Fibrosis

To identify and screen candidate genes involved in liver fibrosis progression, we analyzed a transcriptome microarray dataset of mouse livers after 6 weeks of chronic CCl_4 treatment or normal livers from a public database (Gene Expression Omnibus [GEO] Series accession number GSE207857).[34] We found that the messenger RNA (mRNA) expression levels of GDF15, rather than of other member of GDFs, were markedly decreased in mouse livers after 6 weeks of chronic CCl_4 treatment compared with normal control livers (Figure 1*A*). Correlation analysis indicated that the mRNA expression levels of *GDF15* showed a negative correlation trend with the mRNA expression levels of *Acta2* and *Tgfb1* in GEO databases, even though, due to the low number of samples from mouse models of liver fibrosis, the analysis of correlation was not statistically significant in this database (Figure 1*A*). Similar result was also observed in cirrhosis patients in another public dataset of the GEO database (GSE25097) (Figure 1*B*). To determine whether GDF15 expression is associated with liver disease, we initially examined GDF15 levels in human tissue arrays of different liver diseases by immunohistochemistry. Immunohistochemical analysis revealed that hepatic GDF15 expression was only significantly increased in liver tissues of hepatocellular carcinoma (HCC) compared with normal, fibrotic and cirrhotic human liver tissues (Figure 1*C*). We sought to further evaluate whether GDF15 is related to liver fibrosis, we next examined its expression in 2 mouse liver fibrosis models, chronic CCl_4 injection and DDC diet. The mRNA level of *Gdf15* was significantly downregulated in fibrotic livers from both models, together with upregulation of the hepatic stellate cell (HSC) activation marker *Acta2* (Figure 1*D* and *E*). In addition, immunohistochemical staining of GDF15 revealed that hepatic GDF15 expression was decreased in the cholestasis- and CCl_4-induced fibrosis model (Figure 1*F* and *G*). These data indicate that GDF15 is downregulated in fibrotic livers, raising the possibility that it may play a role in liver fibrosis progression.

GDF15 Deficiency Aggravates Toxin- and Cholestasis-Induced Fibrosis

In order to examine the overall role of GDF15 during liver fibrogenesis in vivo, we generated *Gdf15* knockout (KO) mice via the CRISPR/Cas9 system. GDF15 was undetectable in the livers of *Gdf15* KO mice, indicating successful KO (Figure 2*A* and *B*). *Gdf15* KO mice were normal in appearance and mating. We then investigated fibrogenesis in *Gdf15* KO mice used to generate a toxic fibrosis mouse model induced by chronic CCl_4 treatment. Mice were repetitively exposed to CCl_4 for 4 weeks (2 times/wk). *Gdf15* KO mice displayed significantly increased liver injury and fibrosis, as assessed by hematoxylin and eosin (H&E) and Sirius red staining, compared with corn oil control models (Figure 2*C*–*E*). As expected, the expression of α-smooth muscle actin (α-SMA), a marker of HSC activation, in liver sections strongly increased in *Gdf15* KO mice compared with those in wild-type (WT) mice upon CCl_4-induced fibrogenesis (Figure 2*C* and *E*). We also observed that alanine aminotransferase (ALT) and aspartate aminotransferase (AST) levels in serum and hepatic hydroxyproline content from *Gdf15* KO mice markedly increased compared with those from WT mice after CCl_4 treatment (Figure 2*F* and *G*). Moreover, the hepatic mRNA expression of prototypical profibrotic genes (*Acta2*, *Col1a1*, *Col1a2*, and *Pdgfr*) were also elevated in CCl_4-induced *Gdf15* KO mice (Figure 2*H*). These results indicate that GDF15 absence led to a deterioration of toxin-induced liver fibrosis.

To further analyze the role of GDF15 in liver fibrosis due to other causes, we employed a DDC diet–induced mouse liver fibrosis model, recapitulating clinical features of human biliary fibrosis. After 4 weeks of DDC feeding, the histologic staining of liver sections showed that DDC-fed *Gdf15* KO mice displayed a larger fibrosis area in liver tissue than their WT counterparts (Figure 3*A* and *B*). Moreover, Sirius red staining showed significantly more collagen deposition and fibrous

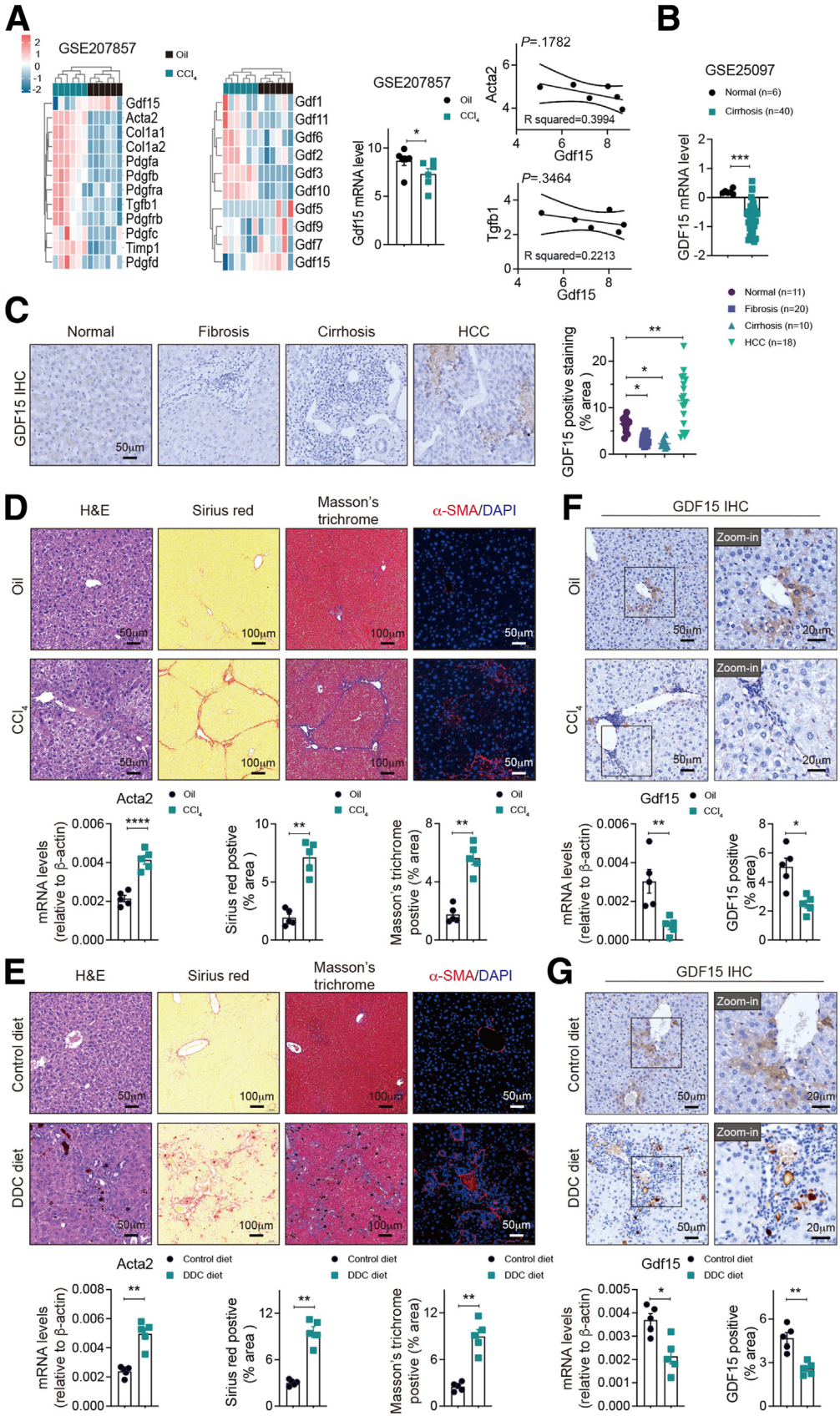

Figure 1. GDF15 expression is decreased in livers from patients and mice with fibrosis or cirrhosis. (*A*) Heatmap of the expression levels of GDF15, fibrosis-related genes, and other GDF members in livers from 6-week CCl_4 model (from GEO at GSE207857, n = 6 mice per group). Correlation analysis between the mRNA expression of *Gdf15* and *Acta2* or *Tgfb1* in liver samples from 6-week CCl_4 model (from GEO at GSE207857, n = 6). (*B*) The mRNA expression level of GDF15 in livers from healthy control individuals (n = 6) and patients with cirrhosis (n = 40, from GEO at GSE25097). (*C*) Representative immunohistochemical staining of GDF15 in a human HCC progression tissue array (DP087Lv01) and its statistical summary. (*D*, *E*) WT mice were treated with 4 weeks of CCl_4 or underwent DDC feeding for 4 weeks. Representative liver histology of H&E staining, Sirius red staining, Masson's trichrome staining, and its quantification. Expression of α-SMA was determined by immunofluorescence. (*F*, *G*) Liver samples from CCl_4 or DDC diet–induced fibrosis models were collected for immunohistochemical staining of GDF15. Representative liver immunohistochemical staining of GDF15 and its mRNA levels were measured by qRT-PCR. Results are displayed as mean ± SEM (n = 5 per group). Statistical significance was assessed by 1-way analysis of variance or Student's *t* test. **P* < .05; ***P* < .01; ****P* < .001; *****P* < .0001.

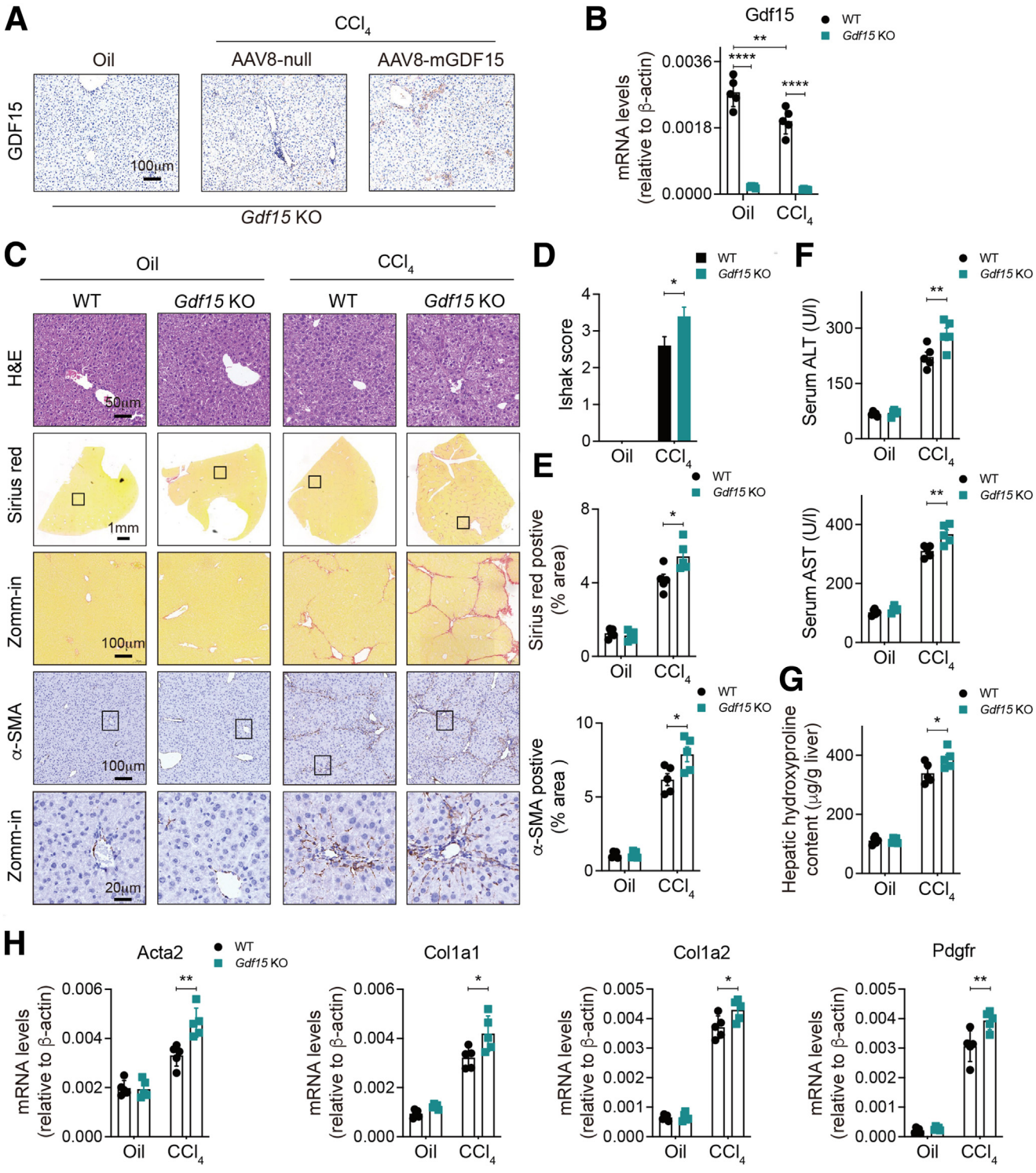

Figure 2. *Gdf15* KO mice exacerbates CCl_4-induced liver fibrosis in mice. (*A–H*) WT and *Gdf15* KO mice underwent 4 weeks of CCl_4-induced liver fibrosis. (*A*, *B*) Representative liver immunohistochemical staining of GDF15 and *Gdf15* mRNA levels were measured by qRT-PCR from WT and *Gdf15* KO mice treated with CCl_4 or vehicle (corn oil). Representative liver histology of (*C*) H&E and Sirius red staining and (*D*, *E*) its quantification. Expression of α-SMA was determined by (*C*) immunohistochemistry and (*E*) its quantification. Serum levels of (*F*) ALT and AST and (*G*) hepatic hydroxyproline content were measured. (*H*) Hepatic mRNA levels of fibrogenic genes (*Acta2*, *Col1a1*, *Col1a2*, and *Pdgfr*) were measured by qRT-PCR. Data are presented as mean ± SEM. $^*P < .05$, $^{**}P < .01$, $^{****}P < .0001$. The *P* value is calculated using 2-way analysis of variance.

connective tissue hyperplasia in liver tissue of *Gdf15* KO mice compared with that of WT control animals (Figure 3*A*). Consistently, *Gdf15* KO mice also showed markedly increased intrahepatic α-SMA expression (Figure 3*A* and *C*). However, serum ALT and AST levels and hepatic hydroxyproline content were compatible between WT and *Gdf15* KO mice (Figure 3*D* and *E*), suggesting that a similar liver injury occurred. We also observed a significant increase in mRNA levels of *Acta2*, *Col1a1*, *Col1a2*, and *Pdgfr* in *Gdf15* KO mice (Figure 3*F*). Taken together, our data clearly revealed that *Gdf15* deficiency aggravated fibrosis in mouse models of toxin- and cholestasis-induced liver fibrosis.

AAV8-Mediated GDF15 Delivery Contributes to Control of Toxin- and Cholestasis-Induced Fibrosis Progression

Furthermore, the effects of GDF15 were examined in toxin- and cholestasis-induced fibrosis models in mice by its overexpression with AAV-medicated gene delivery. Thus, we used AAV8 (a gene vector isolated from rhesus monkeys, which is used to transduce hepatocytes because of its high affinity for liver cells)[35] to overexpress mouse GDF15 in the liver during fibrotic progression. Using this approach, we next examined the consequences of GDF15 overexpression in hepatocytes following AAV8 delivery under conditions of chronic liver damage. 2 weeks after the AAV8 injection, the mice were treated with CCl_4 for another 4 weeks to induce liver fibrosis (Figure 4*A*). *ZsGreen* signals were clearly observed in liver sections after AAV8-ZsGreen injection and *GDF15* transcript was markedly upregulated in AAV8-mGDF15-injected mice liver, indicating efficient transduction of AAV8 vectors (Figure 4*B* and *C*). H&E, Sirius red staining, and Masson's trichrome staining assays showed reduced liver injury and fibrosis elicited by GDF15 overexpression in hepatocytes following AAV8 delivery compared with the effects observed in mice that were injected with AAV8-null (Figure 4*D* and *E*). Accordingly, AAV8-mGDF15 delivery notably reduced α-SMA expression and liver hydroxyproline content in the fibrotic livers, in line with an improved Ishak histological fibrosis score (Figure 4*F*–*H*). Serum levels of ALT and AST were significantly lower in mice that received AAV8-mGDF15 than those mice receiving a control AAV8-null, indicating an improvement in liver function (Figure 4*I*). In addition, hepatic levels of prototypical profibrotic related transcripts (*Acta2*, *Col1a1*, *Col1a2*, and *Pdgfr*) were significantly reduced in mice that received AAV8-mGDF15, compared with those receiving control AAV8-null (Figure 4*J*). The expression of Ki67, a widely used marker for the evaluation of cell proliferation, was detected by immunohistochemistry. CCl_4 injection increased the number of Ki67-positive hepatocytes in liver sections compared with the control group, and mice that received AAV8-mGDF15 further amplified the elevation of Ki67-positive hepatocytes induced by CCl_4 injection compared with that of the group treated with only CCl_4 (Figure 5*A* and *B*), suggesting that GDF15 prominently regulates hepatocyte proliferation and possibly liver regeneration.

To further analyze the protective role of GDF15 overexpression in liver fibrosis due to other causes, we use mice with cholestasis-induced fibrosis (DDC-containing diet). Two weeks after the AAV8 injection, the mice were fed with DDC for another 5 weeks to induce liver fibrosis (Figure 6*A*). Mice that were injected with AAV8-mGDF15 displayed significantly attenuated liver injury and fibrosis, as assessed by H&E, Sirius red staining, and Masson's trichrome staining, compared with the effects observed in mice that were injected with AAV8-null (Figure 6*B* and *C*). Accordingly, administration of AAV8-mGDF15 in mice notably reduced α-SMA expression in the fibrotic livers, in line with an improved Ishak histological fibrosis score (Figure 6*D* and *E*). However, liver hydroxyproline content and serum levels of ALT and AST were compatible between AAV8-mGDF15 and AAV8-null mice, suggesting that similar liver injury occurred (Figure 6*F* and *G*). We also observed a significant reduction in mRNA levels of *Acta2*, *Col1a1*, *Col1a2*, and *Pdgfr* in mice that were injected with AAV8-GDF15 (Figure 6*H*).

Moreover, to evaluate the therapeutic potential of GDF15, we used recombinant murine GDF15 (rmGDF15) treatment in mice from the second week to the fourth week with CCl_4 treatment (Figure 7*A*). Mice treated with rmGDF15 displayed a significant reduction in the Sirius red–positive area, α-SMA expression, Ishak histological fibrosis score, hepatic hydroxyproline content, and serum ALT and AST levels compared with the CCl_4-treated mice (Figure 7*B*–*G*). Consistently, we also found a significant reduction in *Acta2*, *Col1a1*, *Col1a2*, and *Pdgfr* mRNA levels in mice treated with rmGDF15 (Figure 7*H*). Collectively, these results showed that restoration of hepatic GDF15 expression relieves the liver fibrosis progression, suggesting that GDF15 could be a potential target for liver fibrosis treatment.

GDF15 Alleviates Inflammation and Shapes an Anti-Inflammatory Phenotype of Macrophages in Fibrotic Livers

Inflammation is one of the well-established characteristics of liver fibrosis.[1,5] Next, we examined the impact of GDF15 on local inflammation in fibrotic liver tissues. Figure 8*A* shows higher expression levels of IL-1β, IL-6, and TNF-α in fibrotic livers obtained from *Gdf15* KO mice than that of WT control mice. Consistently, serum levels of IL-1β, IL-6, and TNF-α were higher in *Gdf15* KO mice than their littermates (Figure 8*B*). The infiltration of macrophages and neutrophils has been proven to predominantly mediate liver inflammation and induce high levels of circulating proinflammatory cytokines, such as IL-6 and TNF-α. Subsequently, we also evaluated the accumulation of hepatic inflammatory cells by F4/80 (a macrophage marker) and MPO (a neutrophil marker) staining in fibrotic liver tissues. Compared with the WT mice, GDF15 deficiency markedly increased macrophage and neutrophil infiltration in toxin- and cholestasis-induced fibrotic liver tissues (Figure 8*C*–*F*).

Because GDF15 could regulate the progression of liver fibrosis, we hypothesized that GDF15 expression can influence macrophage phenotype switch during hepatic fibrosis.

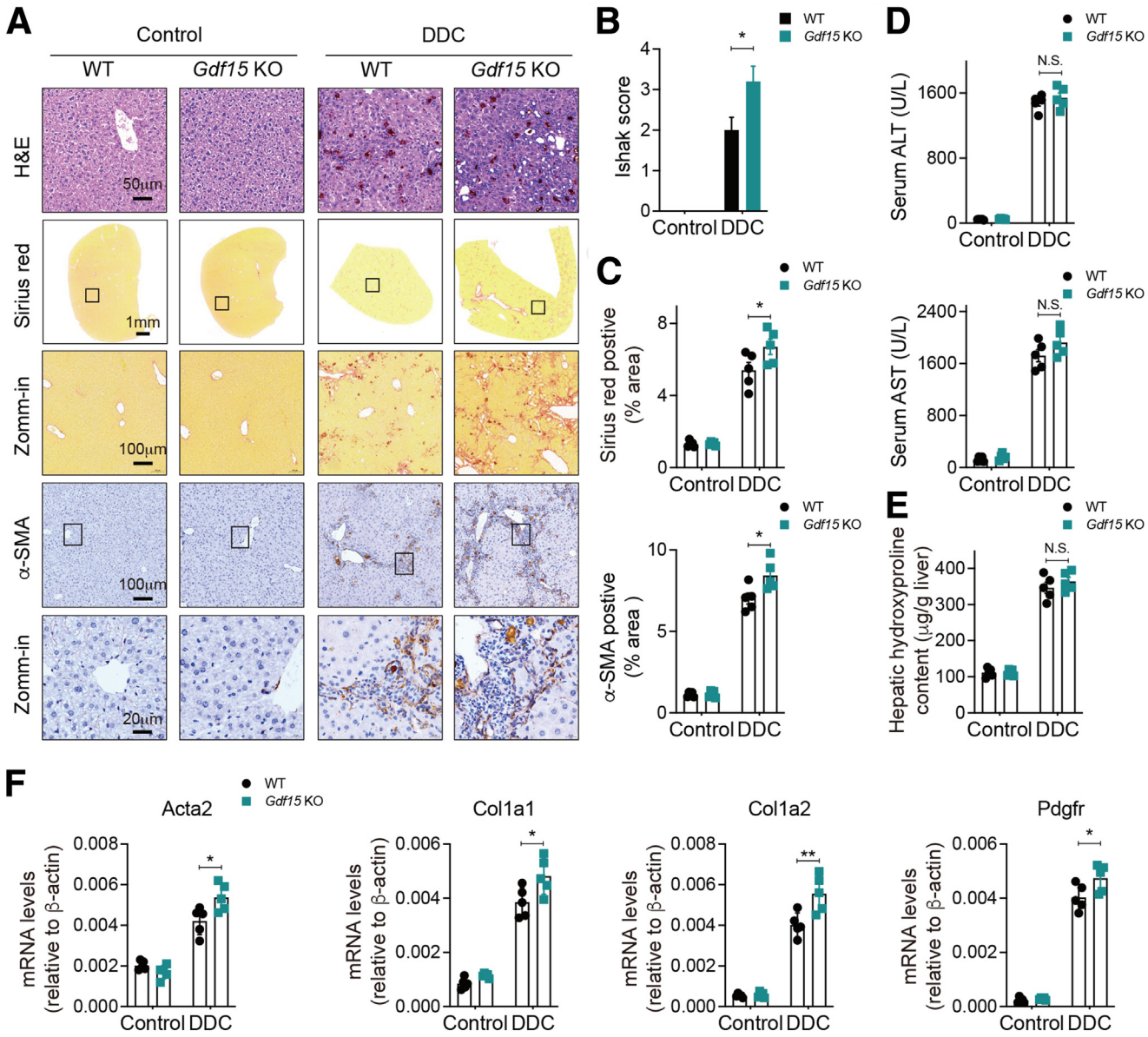

Figure 3. *Gdf15* KO mice exacerbates DDC-diet–induced liver fibrosis in mice. (*A-F*) WT and *Gdf15* KO mice underwent DDC feeding for 4 weeks. Representative liver histology of (*A*) H&E and Sirius red staining and (*B*, *C*) its quantification. Expression of α-SMA was determined by (*A*) immunohistochemistry and (*C*) its quantification. Serum levels of (*D*) ALT and AST and (*E*) hepatic hydroxyproline content were measured. (*F*) Hepatic mRNA levels of fibrogenic genes (*Acta2*, *Col1a1*, *Col1a2*, and *Pdgfr*) were measured by qRT-PCR. Data are presented as mean ± SEM. **P* < .05, ***P* < .01. The *P* value is calculated using 2-way analysis of variance. N.S., no significance.

Murine models revealed that inflammatory Ly6C^{hi} expressing monocytes accumulate in injured liver and are critical for HSC activation, we initially checked this phenotype change in our mouse models. Flow cytometric analysis showed that CCl_4 treatment significantly upregulated the number of Ly6C^{hi} macrophages (gated from CD11b^{high} and F4/80^{intermediate} expression [monocyte-derived macrophages] subset), while in livers of *Gdf15* KO mice, the population of Ly6C^{hi} macrophages was significantly increased after chronic CCl_4 injection (Figure 9*A*). Meanwhile, the number of CD11b^{high} and F4/80^{intermediate} cells was not changed by GDF15 deletion (Figure 9*B*), indicating that GDF15 deletion induces a macrophage phenotype switch from Ly6C^{low} to Ly6C^{hi} during mouse liver fibrosis. Parallel to the intrahepatic macrophages, we also investigated other immune cells, such as B cells (B220$^+$) and T cells (CD3$^+$, CD4$^+$, CD8$^+$), which were not significantly affected in CCl_4-induced WT and *Gdf15* KO liver fibrosis mouse models (Figure 9*C*).

Further, to investigate whether GDF15 deficiency influenced macrophage polarization, we initially analyzed the quantification of M2 macrophages in liver slices, and the results showed that fewer CD68$^+$ CD163$^+$ macrophages were observed in the *Gdf*15 KO mice than in the WT mice

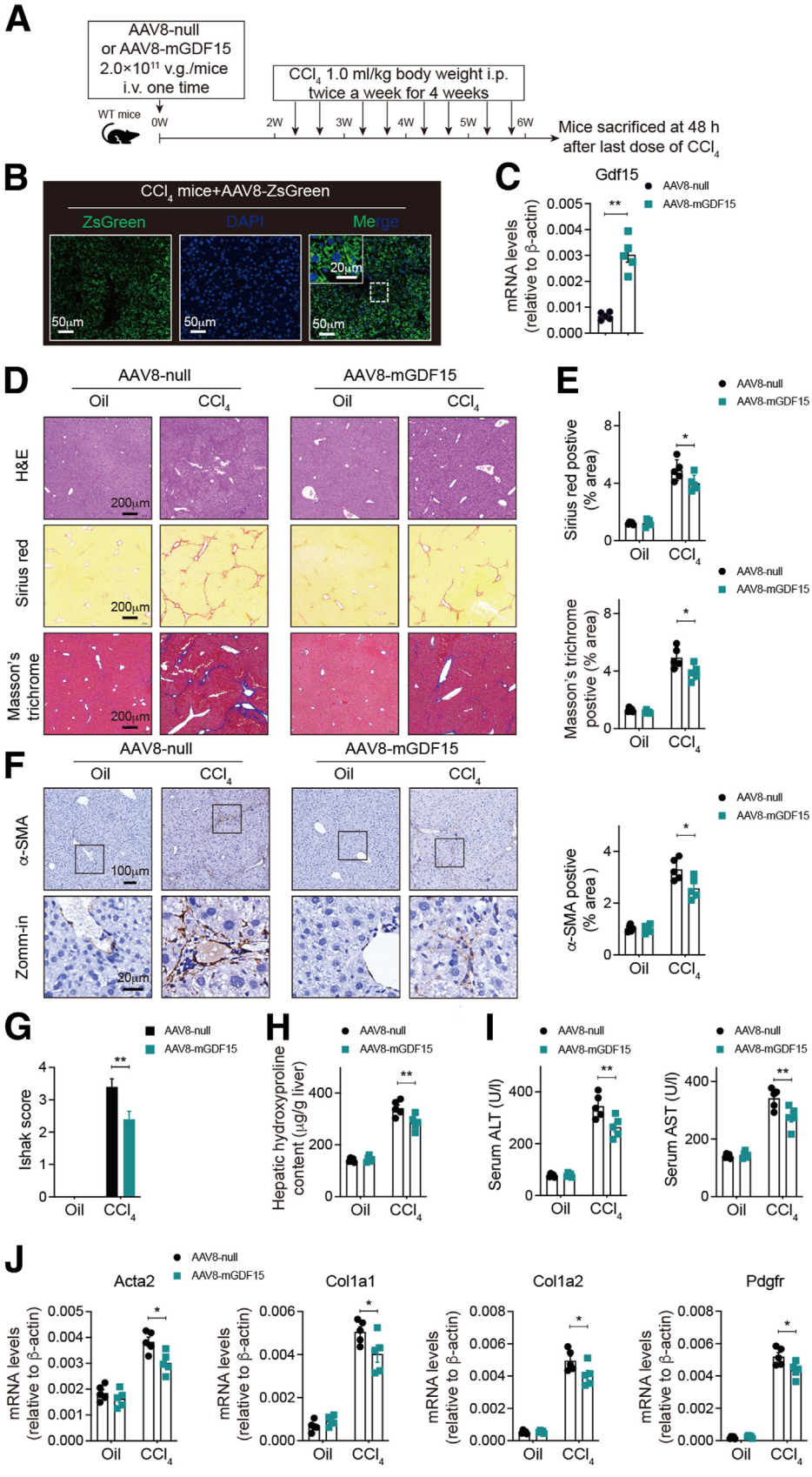

Figure 4. Effect of GDF15 overexpression on CCl_4-induced liver fibrosis in mice by AAV8 vectors. (*A*) Schematic of the experimental design of AAV8 overexpression treatment in WT mice that were treated with CCl_4 for another 4 weeks to induce liver fibrosis. (*B*) AAV8.ZsGreen immunofluorescence in liver samples from CCl_4-treated mice. Scale bar = 50 μm. (*C*) GDF15 expression in liver samples from CCl_4-treated mice was confirmed via qRT-PCR. (*D*, *E*) Representative liver histology of (*D*) H&E, Sirius red, and Masson's trichrome staining and (*E*) its quantification. Expression of α-SMA was determined (*F*) by immunohistochemistry and (*F*, *G*) its quantification. (*H*) Hepatic hydroxyproline content and serum levels of (*I*) ALT and AST were measured. (*J*) Hepatic mRNA levels of fibrogenic genes (*Acta2*, *Col1a1*, *Col1a2*, and *Pdgfr*) were measured by qRT-PCR. Results are displayed as mean ± SEM. $^*P < .05$, $^{**}P < .01$. Statistical significance was assessed by 2-tailed Student's *t* test or 2-way analysis of variance. i.p., intraperitoneal; i.v., intravenous; v.g., vector genomes.

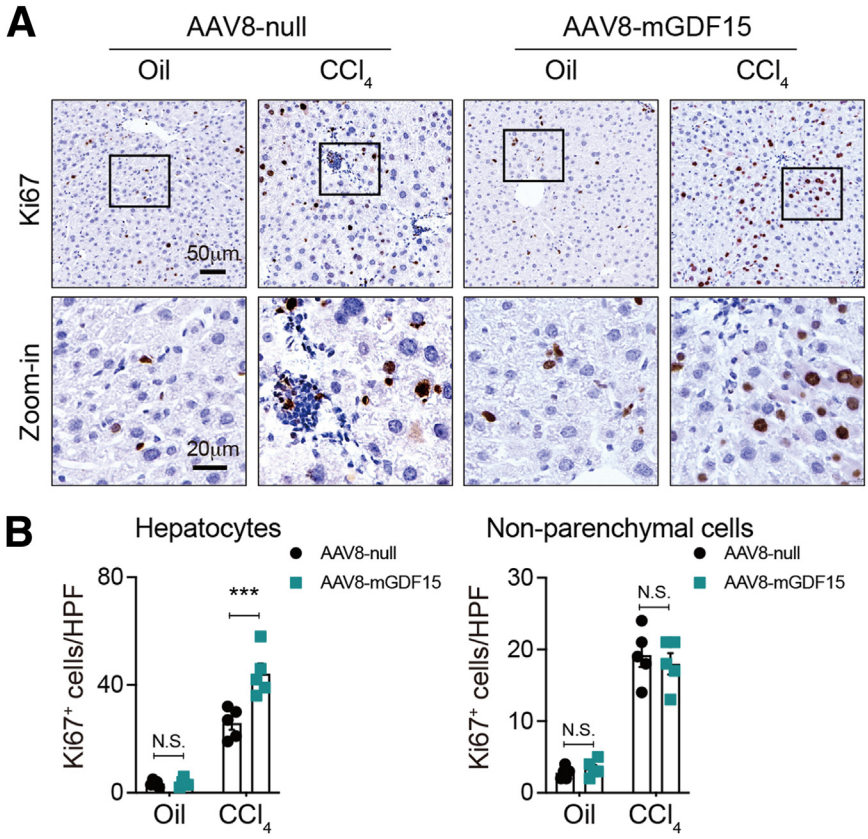

Figure 5. AAV8-mediated restoration of hepatic GDF15 expression increases hepatocyte proliferation in CCl_4-induced fibrosis. (*A*, *B*) Representative photomicrographs of (*A*) Ki67 staining in fibrotic livers of mice injected with AAV8-null or AAV8-mGDF15. (*B*) Quantitative analysis. Results are displayed as mean ± SEM. ***$P < .001$. Statistical significance was assessed using 2-way analysis of variance. N.S., not significant.

after chronic CCl_4 injection or DDC diet (Figure 9*D* and *E*). The nuclear factor κB (NF-κB) pathway is a well-characterized regulatory pathway intensively involved in macrophage-orchestrated acute/chronic liver inflammation.[36] Herein, immunostaining analysis of fibrotic livers also revealed that *Gdf15* KO mice exhibited activated the NF-κB pathway (Figure 9*F*). This finding is consistent with previous studies that increasing GDF15 significantly suppresses activation of keratinocytes by inhibiting the NF-κB pathway.[33] Additionally, we measured expression of macrophage polarization markers in the fibrotic liver by quantitative reverse-transcription polymerase chain reaction (qRT-PCR). Compared with mice that were injected with AAV8-null, mice that received AAV8-mGDF15 expressed lower mRNA levels of *IL-1β*, *TNF-α*, and *NOS2* (M1 marker) but higher mRNA levels of *YM1*, *Arg1* and *CD206* (M2 marker) (Figure 10*A*). Based on these results, we next investigated the direct effect of GDF15 treatment on macrophage polarization ex vivo, using WT bone marrow–derived macrophages (BMDMs). We measured the gene expression of M1/M2 polarization markers in macrophages by qRT-PCR. Significantly decreased expression of the M1 markers (*IL-1β*, *TNF-α*, and *NOS2*) were observed following cell incubation with LPS plus IFN-γ and recombinant GDF15 protein (Figure 10*B*). In contrast, GDF15 upregulated BMDMs expression of the M2 markers (*YM1*, *Arg1*, and *CD206*) following incubation with IL-4 plus IL-13, suggesting that GDF15 promotes macrophage polarization to the anti-inflammatory M2-like phenotype (Figure 10*B*). Macrophage depletion by repeated liposomal clodronate injection efficiently reduced F4/80-positive macrophages and ameliorated liver fibrosis following CCl_4 treatment in both WT and *Gdf15* KO mice (Figure 11*A*–*D*). These data indicate that GDF15 may alleviate liver fibrosis by affecting the hepatic $Ly6C^{hi}$ macrophage population and polarization of macrophages and then the production of anti-inflammatory cytokines.

Metabolic Commitment to OXPHOS Determines the Anti-Inflammatory Memory of GDF15-Preprogrammed Macrophages to Ameliorate Liver Fibrosis

Metabolic reprogramming is key to controlling the inflammatory response in macrophages.[21] An intriguing observation in our study is that the culture medium (containing phenol red) of rmGDF15-treated macrophages appeared to be less acidic than that of untreated macrophages, suggesting that their metabolism was altered by GDF15. Indeed, both glucose consumption and lactate accumulation were decreased in rmGDF15-preprogrammed macrophages (Figure 12*A*). Accordingly, we found that compared with untreated control macrophages, the extracellular acidification rate (ECAR) was significantly reduced and the oxygen consumption rate (OCR) was markedly increased in GDF15-reprogrammed macrophages, resulting

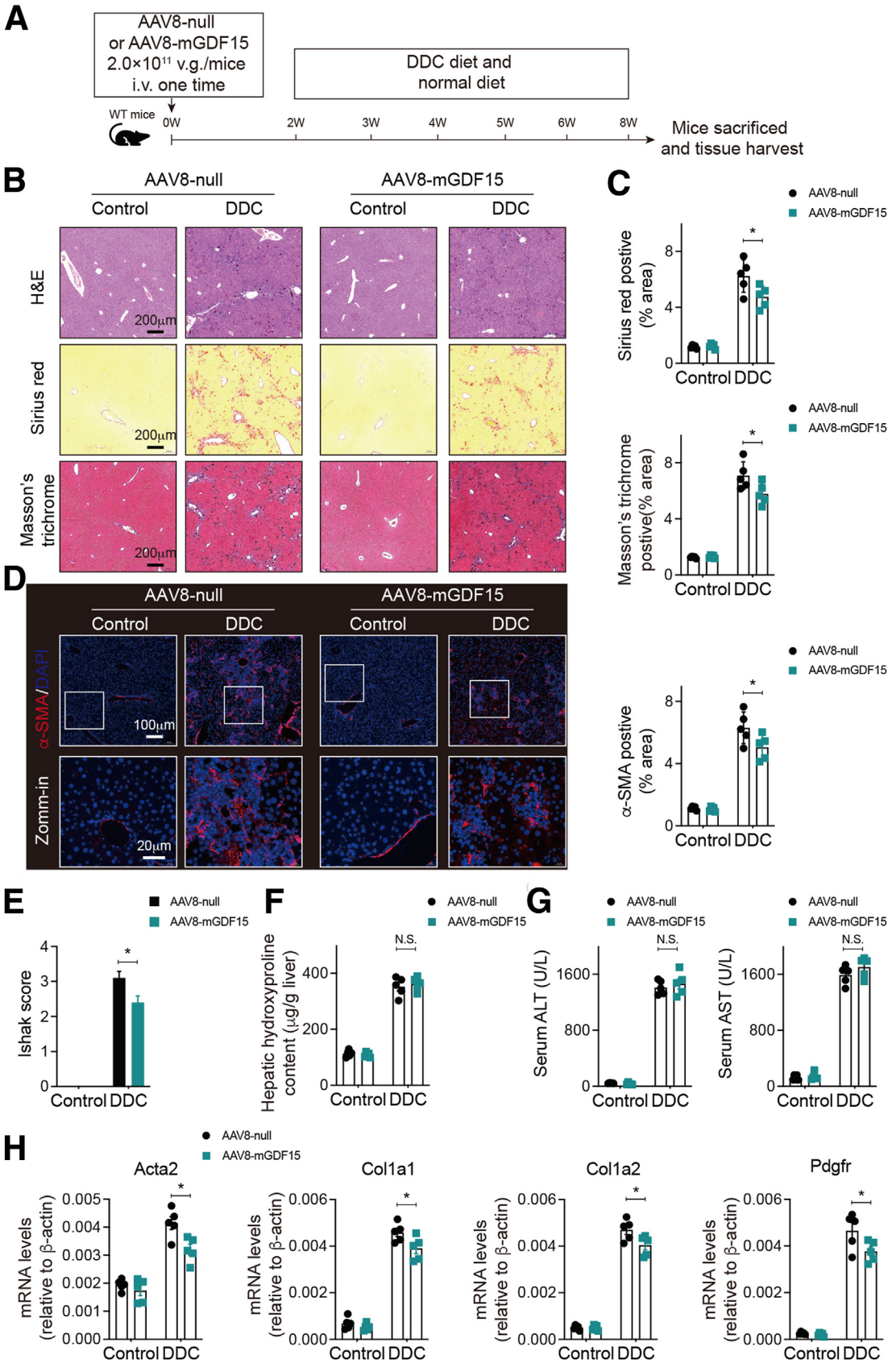
A
AAV8-null
or AAV8-mGDF15
2.0×10^11 v.g./mice
i.v. one time
DDC diet and
normal diet
WT mice
0W
2W
3W
4W
5W
6W
8W
Mice sacrificed
and tissue harvest
B
AAV8-null
AAV8-mGDF15
Control
DDC
H&E
Sirius red
Masson's trichrome
200μm
C
AAV8-null
AAV8-mGDF15
Sirius red postive (% area)
Masson's trichrome postive(% area)
α-SMA postive (% area)
Control DDC
D
α-SMA/DAPI
Zomm-in
100μm
20μm
E
Ishak score
F
Hepatic hydroxyproline content (μg/g liver)
N.S.
G
Serum ALT (U/L)
Serum AST (U/L)
H
Acta2
Col1a1
Col1a2
Pdgfr
mRNA levels (relative to β-actin)

in a higher OCR/ECAR ratio (Figure 12*B* and *C*). Tellingly, GDF15-preprogrammed macrophages showed an increase in the maximal rate of oxygen consumption after supplementation with carbonyl cyanide FCCP, an ionophore that disrupts adenosine triphosphate synthesis by transporting hydrogen ions through the cell membrane before they are used for OXPHOS (Figure 12*B*). Macrophages activated by proinflammatory stimuli, such as LPS, undergo a metabolic switch toward glycolysis and away from OXPHOS, similar to the Warburg effect observed in tumors.[10] Thus, to further elucidate the effect of GDF15 in LPS-activated macrophages, we first measured intracellular levels of OCR and ECAR. Surprisingly, GDF15-preprogrammed macrophages persisted even after LPS stimulation. Although the ECAR in GDF15-preprogrammed macrophages was comparable to that in control macrophages after LPS stimulation, GDF15-preprogrammed macrophages still had a higher OCR/ECAR ratio (Figure 12*D*), suggesting that GDF15 predetermines an irreversible preference for OXPHOS even in the presence of proinflammatory stimulation. To prove whether GDF15 could induce such metabolic reprogramming in macrophages from liver fibrosis, hepatic macrophages were isolated for extracellular flux analysis. Accordingly, macrophages isolated from mice that received AAV8-mGDF15 had significantly enhanced the OCR in intrahepatic macrophages, compared with the effects observed in mice that were injected with AAV8-null (Figure 12*E* and *F*).

To further investigate how GDF15 affects OXPHOS, we initially evaluated the mitochondrial mass in macrophages and found that GDF15-preprogrammed macrophages did not have more mitochondria than control macrophages (Figure 12*G*). Interestingly, GDF15-preprogrammed macrophages did not accumulate mitochondrial reactive oxygen species upon LPS stimulation, suggesting that GDF15 may modulate the activities of mitochondrial complexes (Figure 12*H*). Thus, we examined the enzymatic activities of all 5 mitochondrial complexes and found that compared with mitochondria isolated from control macrophages, those from GDF15-reprogrammed macrophages, upon LPS stimulation, possessed much higher enzymatic activities of mitochondrial complexes I, III, and V, while the enzymatic activities of the other 2 mitochondrial complexes (complexes II and IV) were not affected (Figure 12*I*). Consistently, GDF15-reprogrammed macrophages had a higher mitochondria membrane potential and an elevated adenosine triphosphate/adenosine diphosphate ratio (Figure 12*J*). We then investigated the transcript levels of representative subunits of the mitochondrial complexes in order to test whether GDF15 could directly affect the expression of mitochondrial complexes. We observed that GDF15 induced a significant increase in transcript levels of complex I (I-*Ndufa7*), III (III-*Uqcr11*), and V (V-*Atp5j2*) subunits in macrophages upon LPS stimulation, while mRNA levels of complex II (II-*Sdhc*) and complex IV (IV-*Cox7c*) were not affected (Figure 12*K*). Taken together, these data suggest that elevation of GDF15 expression occurs together with an alteration in the abundance of OXPHOS complexes.

Infiltrating, proinflammatory macrophages dominate the liver macrophage pool and actively contribute to disease progression and fibrosis.[16,18,36] While the inhibition of infiltrating macrophages attenuates the fibrotic response, the transfer of anti-inflammatory macrophages effectively reduces liver fibrosis in mice.[37] To test whether GDF15-preprogrammed macrophages were imprinted with anti-inflammatory abilities, and not hepatocytes or other noninflammatory cells, during the liver response to toxin-induced injury in vivo, we established a mouse model of liver fibrosis by intraperitoneal injection of CCl_4. Subsequently, mice were infused with GDF15-preprogrammed macrophages or control macrophages (1×10^6 cells/mouse) via tail vein 24 hours after the eighth injection of CCl_4 (Figure 13*A*) as described.[37] The mice were continually injected with CCl_4 for another 2 weeks. We found that liver fibrosis was markedly lower in the GDF15-preprogrammed macrophage–recipient mice than in the control macrophage–recipient mice, as revealed by Sirius red and α-SMA staining (Figure 13*B*). In addition, lower serum ALT and AST levels were detected in GDF15-preprogrammed macrophage–recipient mice (Figure 13*C*). Moreover, the expression levels of IL-1β, IL-6, and TNF-α were markedly lower in liver tissues from the GDF15-trained macrophage–recipient mice than that in control mice (Figure 13*D*). These results suggested that infusion of GDF15-preprogrammed macrophages protected against CCl_4-induced liver fibrosis in mice.

To further investigate the effect of macrophages isolated from *Gdf15* KO mice on HSC activation, different types of conditional media (CM) collected from cultured BMDMs were cocultured with LX-2 (a human HSC line with key features of activated HSCs despite limitations due to immortalization). Considering that for in vitro studies, simply culturing HSCs with CM from macrophages can hardly induce their activation, we thus treated HSCs with low-dose recombinant human TGF-β1 to mimic in vivo fibrotic conditions. In the presence of TGF-β1, *Gdf15* KO BMDM-CM treatment significantly promoted HSC activation, as reflected by the upregulation of the α-SMA fluorescence intensity and mRNA levels of *ACTA2* and *COL1A1* (Figure 14*A* and *B*). However, compared with the CCl_4-induced WT mice, terminal deoxynucleotidyl transferase–mediated deoxyuridine triphosphate nick-end

Figure 6. (*See previous page*). AAV8-mediated GDF15 delivery inhibits DDC-diet–induced liver fibrosis. (*A*) Schematic of the experimental design of AAV8 overexpression treatment in WT mice that were fed with DDC for another 4 weeks to induce liver fibrosis. (*B*, *C*) Representative liver histology of (*B*) H&E, Sirius red, and Masson's trichrome staining and (*C*) its quantification. Expression of α-SMA was determined (*D*) by immunofluorescence staining and (*D*, *E*) its quantification. (*F*) Hepatic hydroxyproline content and serum levels of (*G*) ALT and AST were measured. (*H*) Hepatic mRNA levels of fibrogenic genes (*Acta2*, *Col1a1*, *Col1a2*, and *Pdgfr*) were measured by qRT-PCR. Results are displayed as mean ± SEM. $^*P < .05$. Statistical significance was assessed by 2-way analysis of variance. i.v., intravenous; N.S., no significance; v.g., vector genomes.

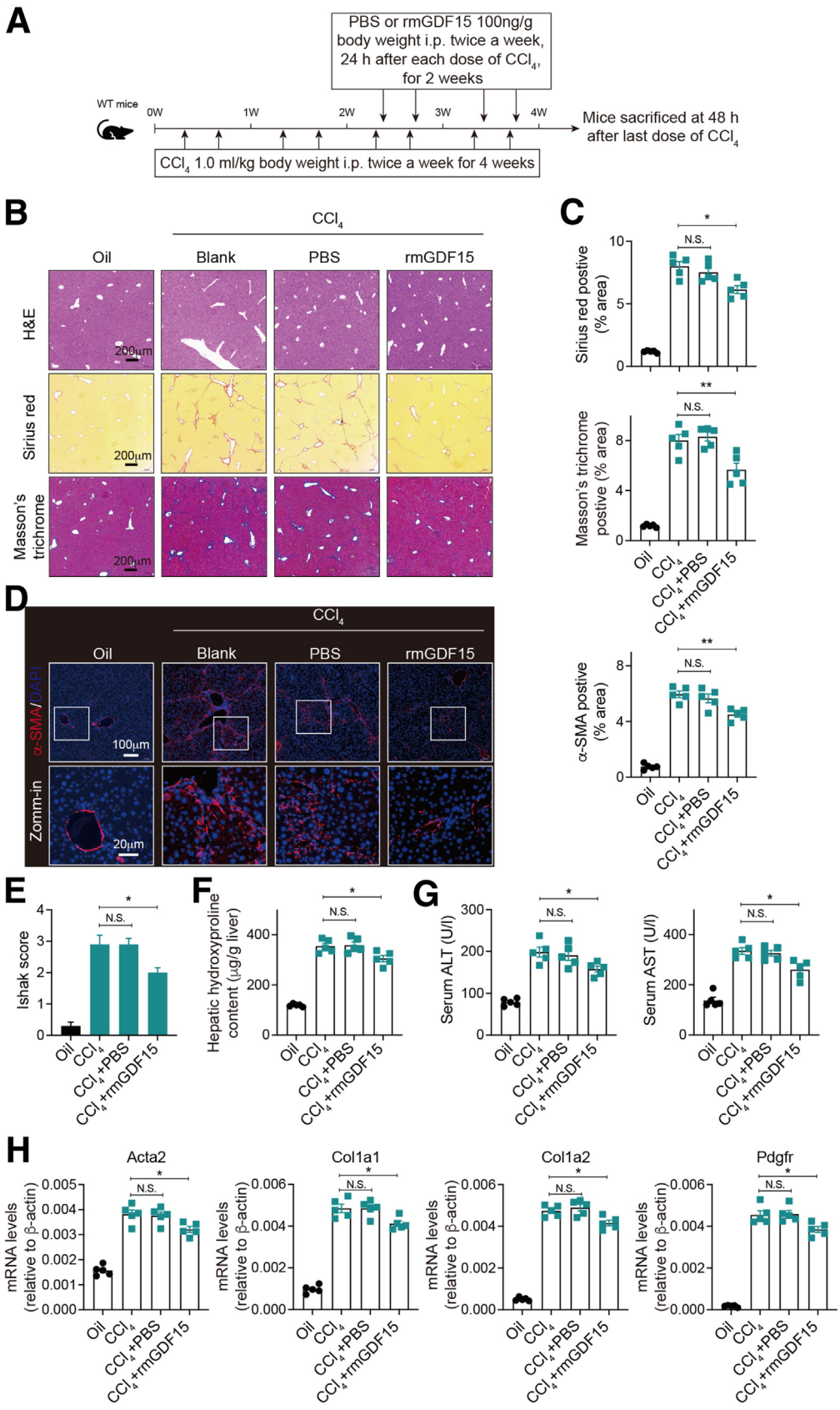

Figure 7. Therapeutic effects of rmGDF15 treatment on established liver fibrosis induced by CCl_4. (*A*) Schematic of the experimental design of phosphate-buffered saline (PBS) or rmGDF15 treatment in WT mice. (*B*, *C*) Representative liver histology of (*B*) H&E, Sirius red staining and (*C*) its quantification. Expression of α-SMA was determined (*D*) by immunofluorescence staining and (*D*, *E*) its quantification. (*F*) Hepatic hydroxyproline content and serum levels of (*G*) ALT and AST were measured. (*H*) Hepatic mRNA levels of fibrogenic genes (*Acta2*, *Col1a1*, *Col1a2*, and *Pdgfr*) were measured by qRT-PCR. Data are displayed as mean ± SEM. $^*P < .05$, $^{**}P < .01$. Statistical significance was assessed by 1-way analysis of variance. i.p., intraperitoneal; N.S., no significance.

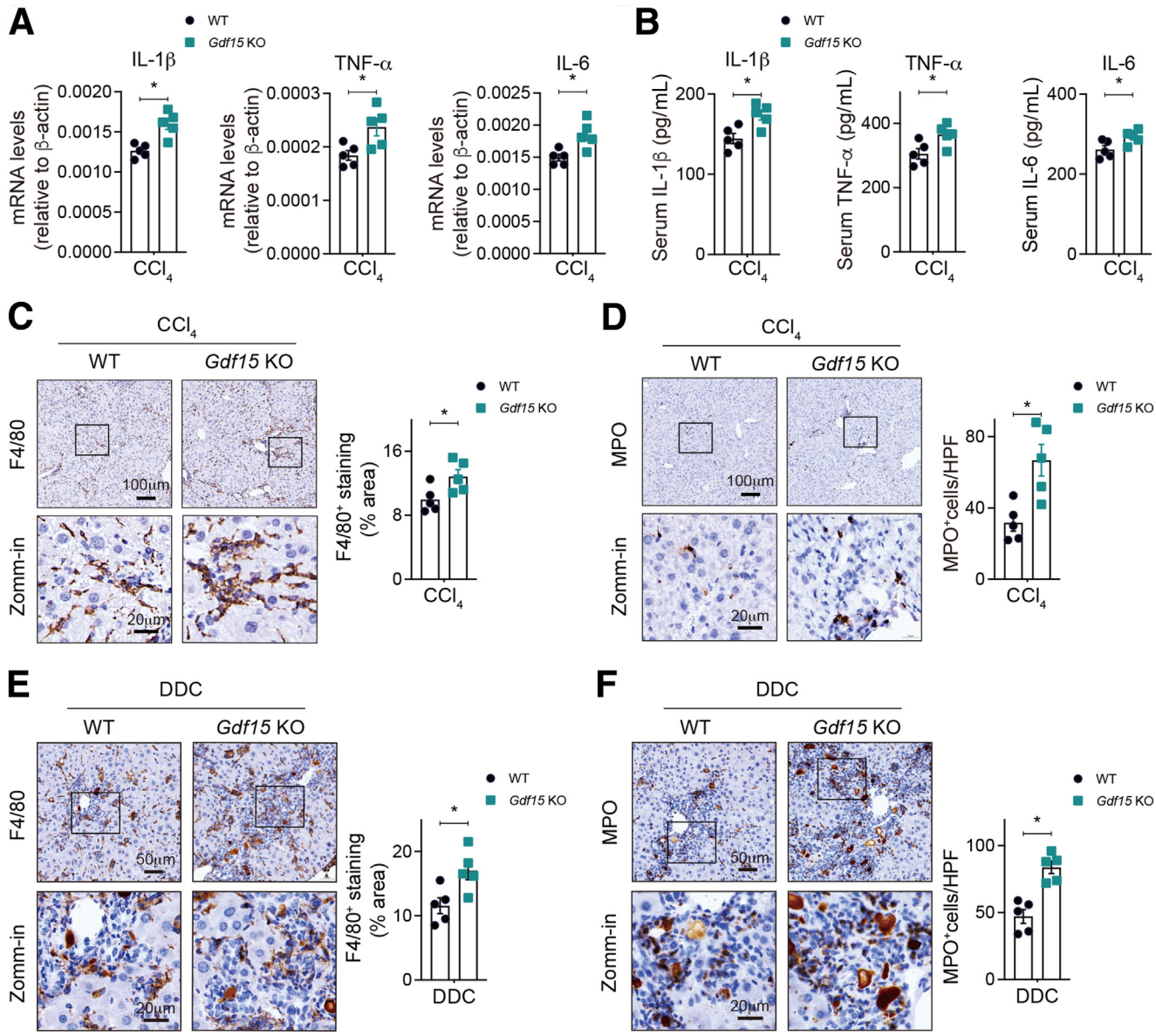

Figure 8. GDF15 attenuates inflammation in mice fibrotic livers. WT and *Gdf15* KO mice underwent 4 weeks of CCl_4-induced liver fibrosis. (*A*) The mRNA expression level of TNF-α, IL-1β, and IL-6 was quantified in liver tissues; (*B*) serum TNF-α, IL-1β, and IL-6 were measured by ELISA. Representative immunohistochemistry staining of (*C*) F4/80 and (*D*) MPO in mice fibrotic livers and quantified as numbers of positive cells per high-power field (HPF). (*E*, *F*) WT and *Gdf15* KO mice underwent DDC feeding for 4 weeks. Representative immunohistochemistry staining of (*E*) F4/80 and (*F*) MPO in mice fibrotic livers and quantified as numbers of positive cells per HPF. Results are displayed as mean ± SEM. $^*P < .05$. Statistical significance was assessed by Student's *t* test.

labeling (TUNEL) and immunohistochemical double immunolabeling demonstrated that the apoptosis of α-SMA–positive HSCs were not significantly affected in the livers of CCl_4-induced *Gdf15* KO mice (Figure 14*C*). These results suggested that *Gdf15* deficiency also promotes liver fibrosis through promoting the activation of HSCs, rather than through inhibiting their apoptosis.

Discussion

Liver fibrosis and its end-stage cirrhosis represent major health problems worldwide, and treatment options to effectively target late-stage liver disease are lacking.[3] Early fibrosis becomes problematic and clinically relevant when dysregulated and excessive scarring occurs in response to persistent injury and leads to altered tissue function, eventually becoming cirrhotic.[1,2,5] Earlier studies regarding GDF15 mainly focused on its function in obesity, diabetes, and cardiovascular diseases.[25,32] However, the role of GDF15 in the pathogenesis of liver fibrosis is largely unknown. In the current study, we have made novel findings toward a better understanding of GDF15 function in the liver microenvironment. We first discovered that GDF15

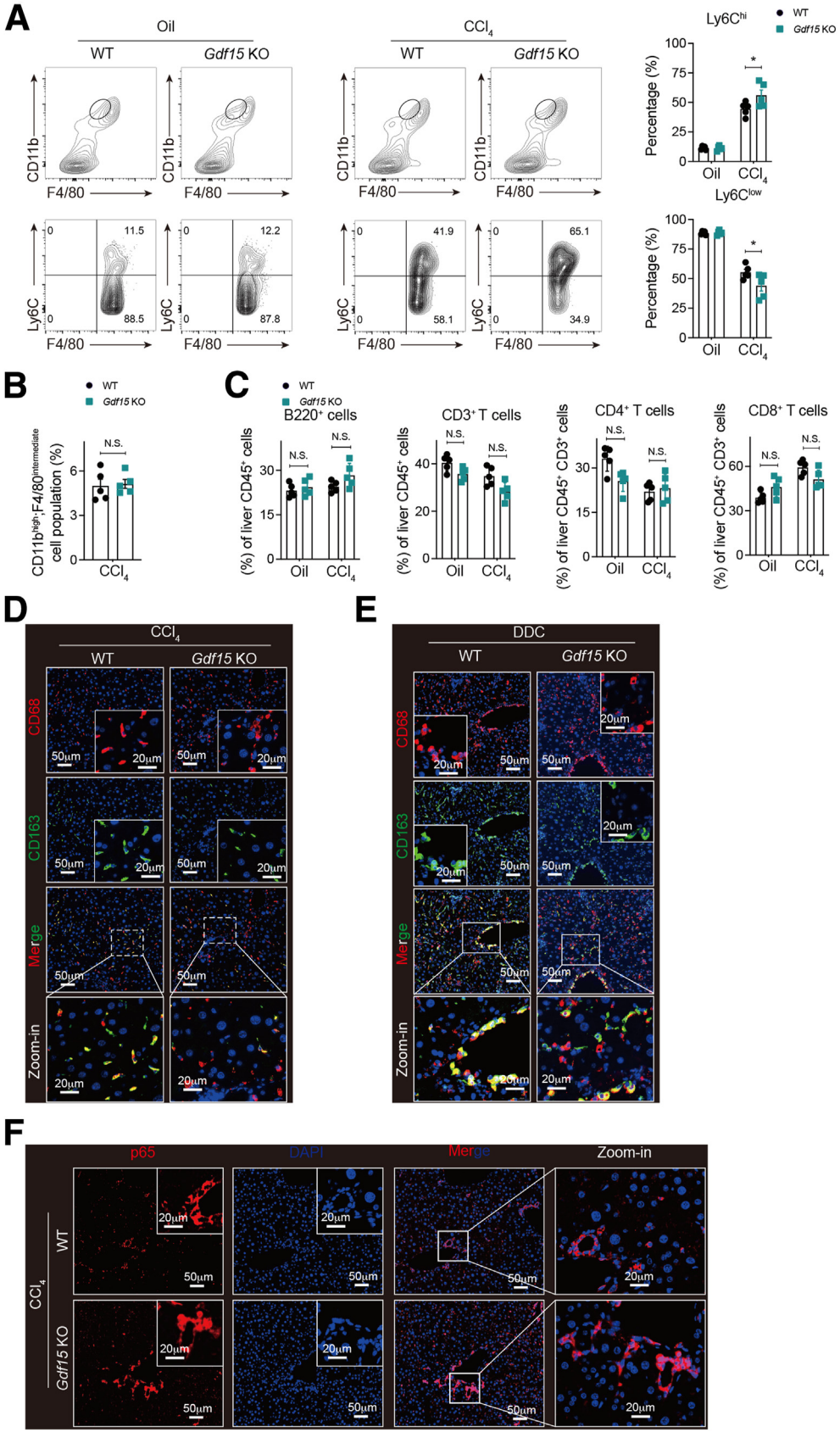

Figure 9. GDF15 controls macrophage phenotype switch and NF-κB pathway activation in mice fibrotic livers. (*A*) Representative images of flow-cytometric analysis of hepatic macrophages from WT and *Gdf15* KO mice after CCl_4-induced fibrotic livers; recruited macrophages ($CD11b^{hi}$ and $F4/80^{Intermediate}$) were further subdivided into $Ly6C^{hi}$ and $Ly6C^{low}$ and its quantification. WT and *Gdf15* KO mice were treated with 4 weeks of CCl_4. Hepatic nonparenchymal cells were stained and analyzed by flow cytometry. (*B*) Percentage of the $CD11b^{hi}$ and $F4/80^{Intermediate}$ expressed cells in liver tissues of WT and *Gdf15* KO mice after CCl_4 injection for 4 weeks (n = 5 mice per group). (*C*) Percentage of the B cells ($B220^+$) and T cells ($CD3^+$, $CD4^+$, $CD8^+$) in liver tissues of WT and *Gdf15* KO mice after CCl_4 injection for 4 weeks (n = 5 mice per group). (*D*, *E*) Dual immunofluorescence staining of CD163 and CD68 in WT and *Gdf15* KO mice fibrotic livers induced by toxin and cholestasis. (*F*) Immunofluorescence staining of p65 and DAPI in liver tissues. Results are displayed as mean ± SEM. $^*P < .05$. Statistical significance was assessed by 2-way analysis of variance or Student's *t* test. N.S., no significance.

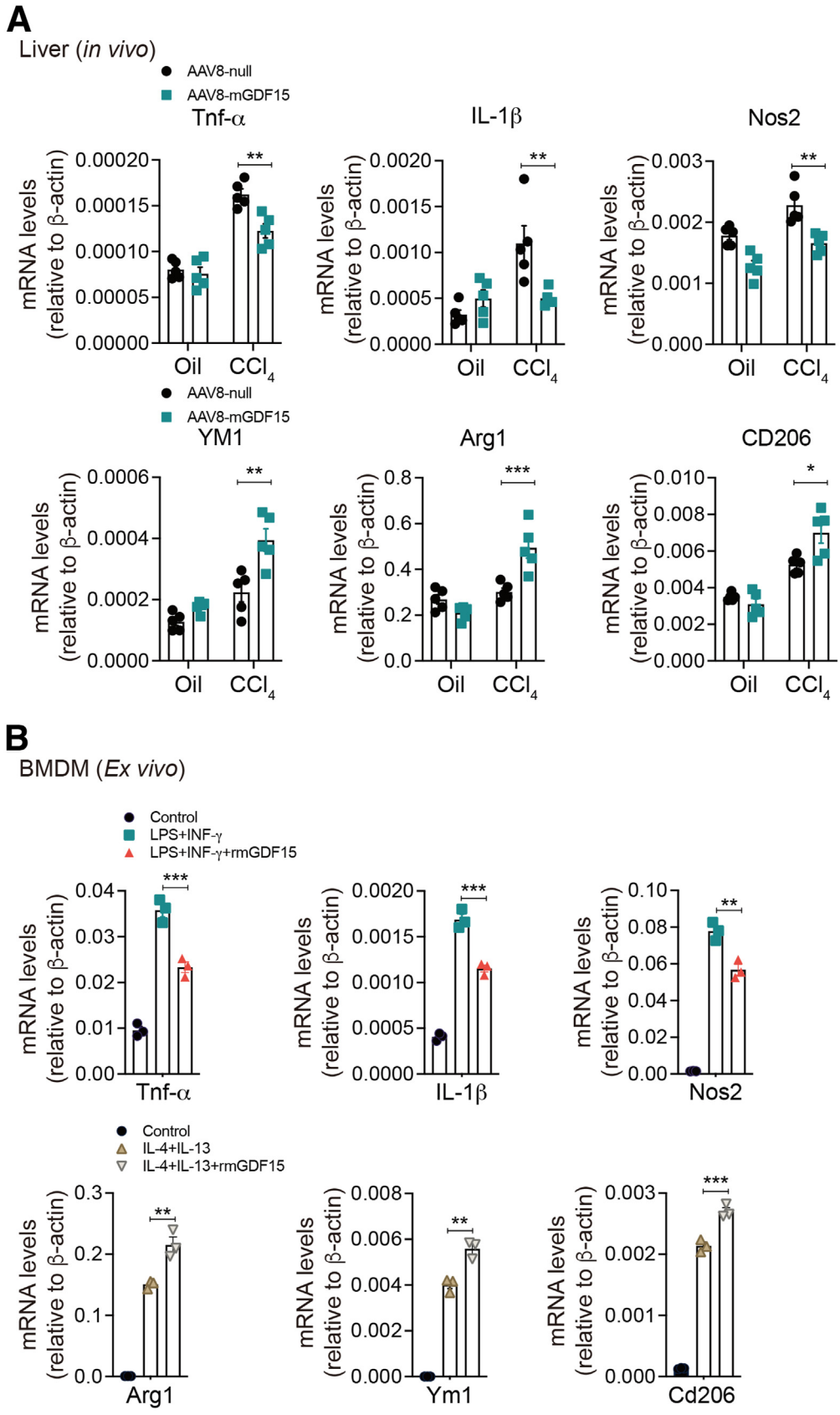

Figure 10. Effects of GDF15 on macrophage polarization. (*A*) The mRNA levels of M1 (*Tnf-α*, *IL-1β*, and *Nos2*) and M2 (*Ym1*, *Arg1*, and *Cd206*) macrophage markers in the liver were measured by qRT-PCR. (*B*) BMDMs from WT mice were either untreated (control) or stimulated with LPS + IFN-γ or IL-4+IL-13 or recombinant mouse GDF15 protein. The mRNA levels of M1 and M2 macrophage markers were analyzed by qRT-PCR. Results are displayed as mean ± SEM. $^{*}P < .05$, $^{**}P < .01$, $^{***}P < .001$. Statistical significance was assessed by 2-way analysis of variance or 1-way analysis of variance.

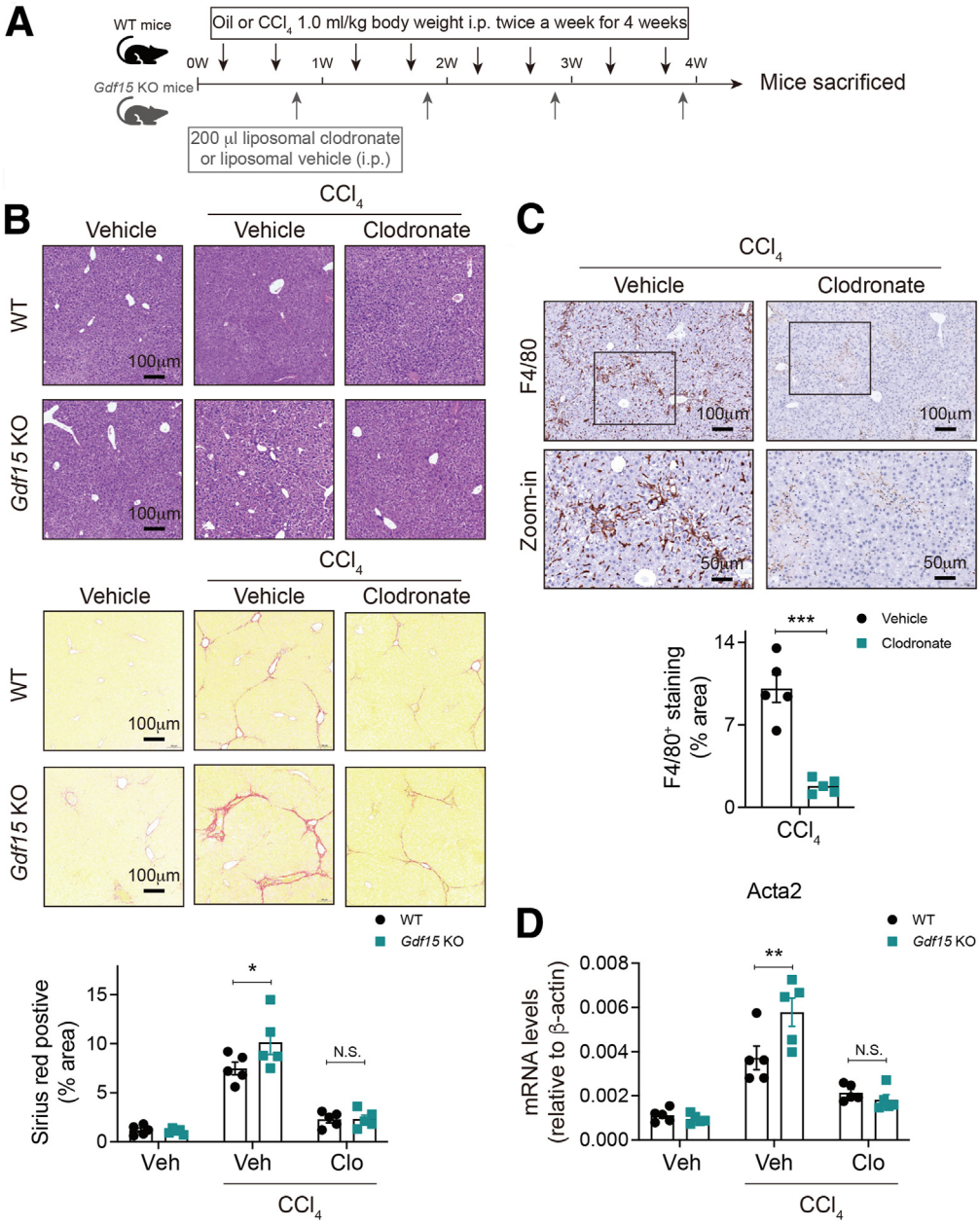

Figure 11. Macrophage deletion reduces CCl_4-induced liver fibrosis in both WT and *Gdf15* KO mice. (*A*) Mice received clodronate or vehicle injections during CCl_4-induced hepatic fibrosis in WT and *Gdf15* KO mice as depicted. (*B*) Representative liver histology of H&E, Sirius red staining and its quantification. (*C*) Depletion of F4/80-positive liver macrophage was confirmed by F4/80 immunohistochemistry. (*D*) Hepatic mRNA level of fibrogenic gene *Acta2* was measured by qRT-PCR. Results are displayed as mean ± SEM. $^{*}P < .05$, $^{**}P < .01$, $^{***}P < .001$. Statistical significance was assessed by 2-way analysis of variance or Student's *t* test. i.p., intraperitoneal; N.S., no significance.

levels decrease markedly in the liver upon hepatic fibrogenesis. Genetic deficiency of GDF15 exacerbates liver fibrotic pathologies in cholestasis-induced and hepatotoxin-induced mouse liver fibrosis models, which is abolished by GDF15 overexpression in hepatocytes following AAV8 delivery. One of the underlying mechanisms is that GDF15 exerts its effects by metabolic reprogramming macrophages to acquire OXPHOS-dependent anti-inflammatory functional fate, reduces proinflammatory mediator expression and macrophage and neutrophil recruitment, and alleviates liver fibrosis. Hence, GDF15 expression and its association with macrophages control hepatic fibrosis by suppressing inflammatory macrophage infiltration, M1 polarization, and proinflammatory cytokine secretion, implying that GDF15 might serve as a bona-fide regulator of liver fibrosis progression and potential targets for anti-hepatic fibrosis therapies.

Uncontrolled inflammation in the liver initiated by resident macrophage activation and massive leukocyte accumulation is a major driving force that transforms self-limited tissue repair processes to a vicious cycle, boosting the progression of liver fibrosis.[1,6,7] Total hepatic macrophages, consisting of liver resident Kupffer cells and monocyte-derived macrophages, contribute to maintaining homeostasis of the liver as well as the progression of acute or chronic liver injury.[9–11] Macrophages are not only crucial to wound healing processes, but can also orchestrate disease progression in rodent models of liver injury.[38] The

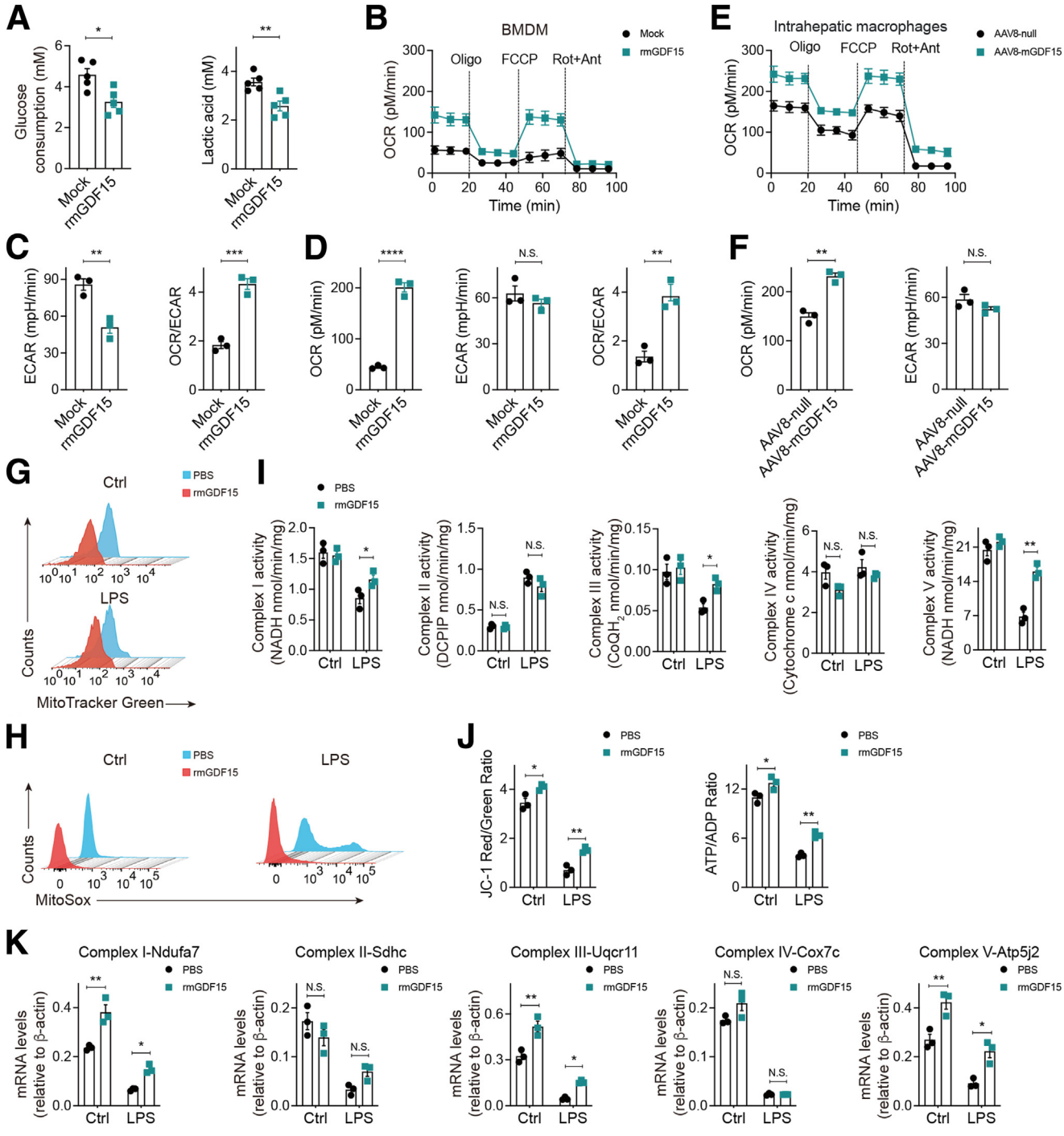

Figure 12. GDF15 preprograms macrophages to commit OXPHOS that shapes an anti-inflammatory phenotype. (*A*) Analysis of 24 hours glucose consumption and lactate production in the supernatant of control or rmGDF15-preprogrammed macrophages (n = 5 per group). (*B*) Extracellular flux analysis of BMDMs (n = 3 per group). (*C*) ECAR of macrophages at the basal condition was detected, and the ratio of OCR to ECAR was calculated. (*D*) Upon activation with LPS for 24 hours, the basal levels of OCR and ECAR of phosphate-buffered saline (PBS) or rmGDF15-treated macrophages were measured, and the ratio of OCR to ECAR was calculated. (*E*, *F*) Two weeks after the AAV8-null or AAV8-mGDF15 injection, the mice were treated with CCl_4 for another 4 weeks to induce liver fibrosis. Mice were sacrificed at 48 hours after last dose of CCl_4. Macrophages were isolated from liver of fibrosis mice using magnet beads and seeded in poly-D-lysine coated Seahorse XF24 cell culture microplates for extracellular flux analysis. (*G*) The accumulation of mitochondrial reactive oxygen species in macrophages was measured by MitoSox Red. (*H*) The mitochondria mass was measured by MitoTracker Green. (*I*) The enzymatic activities of mitochondrial electron transport chain complexes I, II, III, IV, and V of macrophages were determined with or without LPS stimulation (100 ng/mL, 24 hours). (*J*) Resting and activated (LPS 100 ng/mL, 48 hours) macrophages were subjected to JC-1 staining to determine the percentages of JC-1 Red negative cells and JC-1 Red/Green ratio. Macrophage adenosine triphosphate/adenosine diphosphate ratio at steady status or upon LPS stimulation (100 ng/mL, 48 hours) were also measured. (*K*) The mRNA levels of OXPHOS complex subunits I–V in macrophages at steady status or upon LPS stimulation were measured by qRT-PCR. Data are represented as mean ± SEM. $^{*}P < .05$; $^{**}P < .01$; $^{***}P < .001$; $^{****}P < .0001$. Statistical significance was assessed by 2-tailed Student's *t* test or 2-way analysis of variance. i.p., intraperitoneal; i.v., intravenous; N.S., not significant.

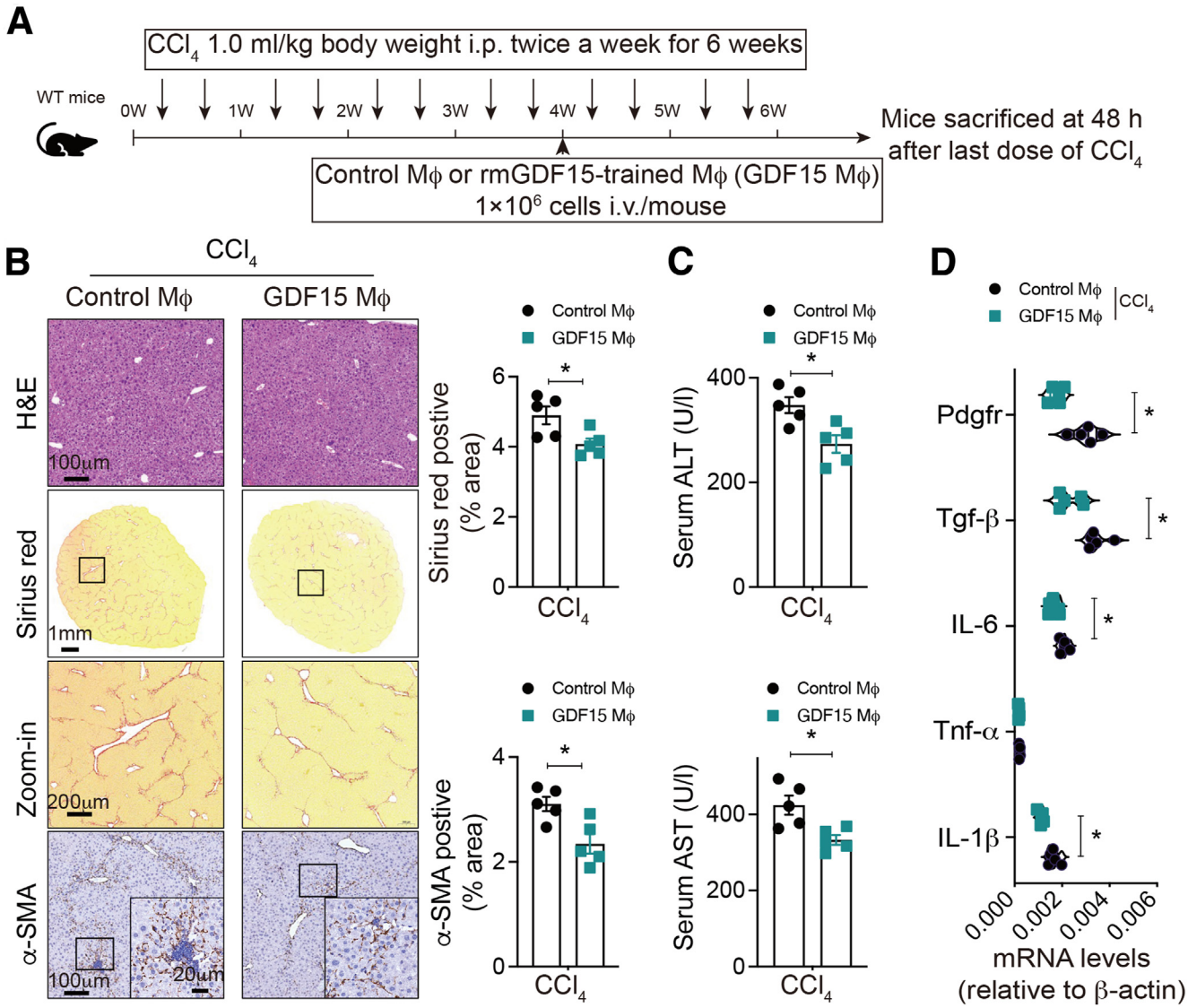

Figure 13. Administration of GDF15-preprogrammed macrophages to mice with liver fibrosis potently alleviates the disease. (*A*) Schematic representation of the experimental procedure. Mice were injected intraperitoneal with CCl_4 twice per week for 6 weeks, and mice were infused with GDF15-preprogrammed macrophages or control (1×10^6 cells/mouse) via tail vein 24 hours after the eighth injection of CCl_4. The mice were continually injected with CCl_4 for another 2 weeks. (*B*) Representative liver histology of H&E, Sirius red staining, and expression of α-SMA was determined by immunohistochemistry and its quantification. (*C*) Serum levels of ALT and AST were measured. (*D*) Hepatic mRNA levels of several genes (*TNF-α*, *IL-1β*, *IL-6*, *TGF-β*, and *Pdgfr*) were measured by qRT-PCR. Results are displayed as mean ± SEM. *$P < .05$. Statistical significance was assessed by 2-way analysis of variance or Student's *t* test.

opposing roles of macrophages in liver disease may be explained by their heterogeneity. Activated macrophages are generally divided into 2 categories, namely, classic M1 and alternative M2, which can be further differentiated into diverse subtypes, each induced by different molecules and eliciting different signals.[14] During the early stages of liver injury, bone marrow–derived monocytes are recruited to the liver and differentiate into M1 macrophages. M1 macrophages can rapidly switch to an M2 phenotype and mediate tissue repair in case of cessation of liver injury.[36] GDF15 is widely regarded as an anti-inflammatory gene possibly involved in macrophage polarization.[39,40] Our data showed that GDF15 is powerful in shaping the anti-inflammatory inclination of maturing macrophages and thus provided a novel strategy for limiting hepatic inflammation and fibrosis by setting the OXPHOS preference of macrophages. Tellingly, in the fibrotic liver, macrophages often express markers of inflammation or resolution simultaneously.[12,16] This suggests that in vivo studies of the heterogeneity of hepatic macrophages would be complex and the conventional classification such as M1 and M2 may not always be suitable. Thus, further classification and evaluation of macrophage functions after rmGDF15 treatment are required to understand how GDF15 mediates its

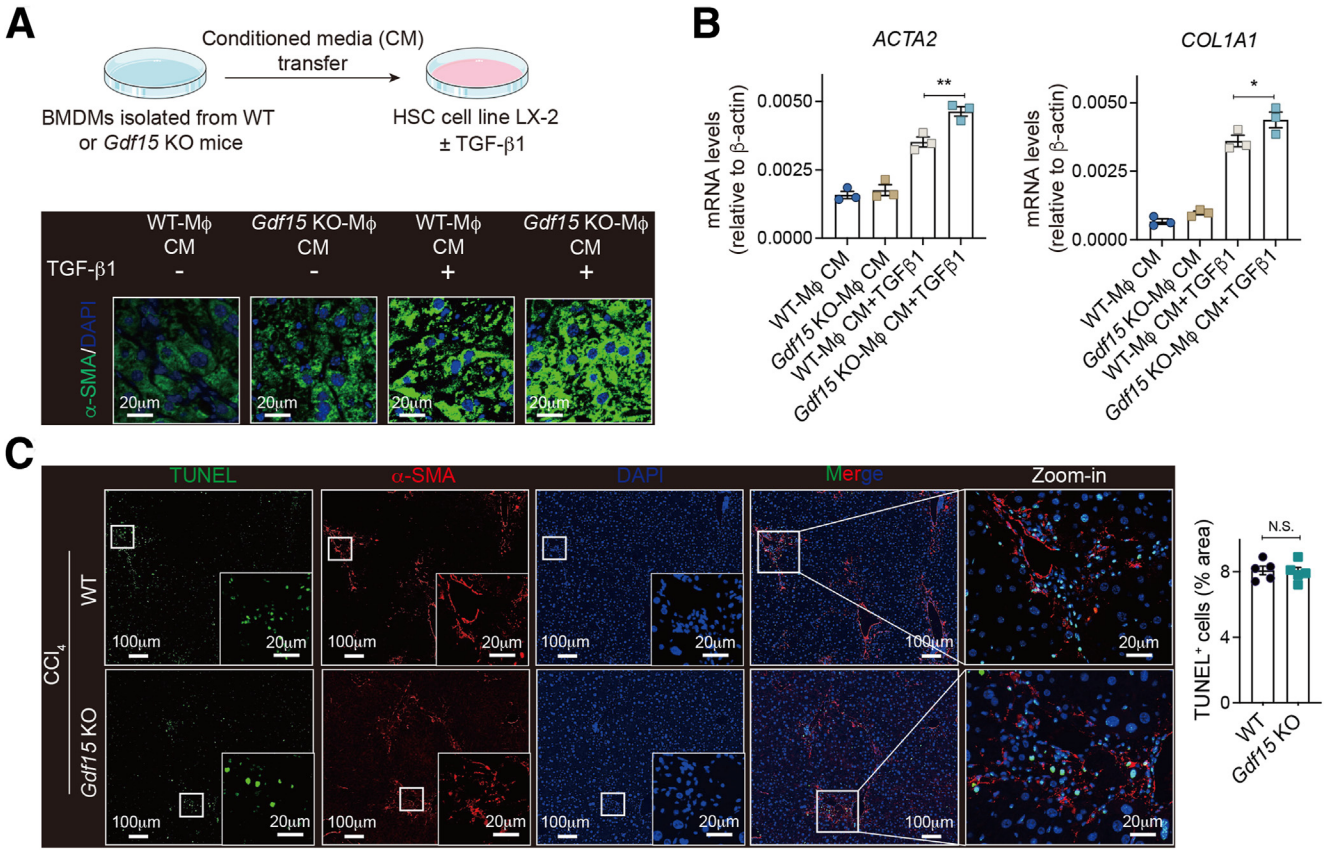

Figure 14. CM collected from *Gdf15* KO BMDMs significantly promotes HSC activation, not apoptosis. (*A*) Schematic drawing showing that LX-2 cells were treated with CM of WT BMDMs and *Gdf15* KO BMDMs in the absence or presence of TGF-β1 for 24 hours. Immunofluorescence staining for α-SMA (green) in treated LX-2 cells. (*B*) The expression levels of *ACTA2* and *COL1A1* in treated LX-2 cells were examined using qRT-PCR. n = 3 per group. (*C*) Representative immunofluorescence images (left) of a-SMA (red) and TUNEL (green) from WT and *Gdf15* KO mice treated with 4 weeks of CCl_4 and its quantification (right). *$P < .05$; **$P < .01$. by 1-way analysis of variance or Student's *t* test. N.S., not significant.

antifibrotic effect through macrophage modulation. Other unknown mechanisms may further contribute to the antifibrotic properties of GDF15. Moreover, in our study, we also showed that GDF15 deficiency promoted hepatic macrophages to change their phenotype from Ly6C^{low} to Ly6C^{hi} in fibrotic mouse livers because Ly6C^{hi} macrophages are key mediators of hepatic fibrosis progression, suggesting that GDF15 regulates macrophage phenotype switch to exert its function in liver fibrosis. Noticeably, chronic liver inflammatory responses are central elements in the development of fibrosis and are principally mediated by the recruited proinflammatory Ly6C^{hi} macrophages, which means that GDF15 may act as an effective therapeutic approach against inflammation during hepatic fibrosis, and the mechanisms of GDF15 in regulating inflammation are closely related with the phenotype switch of macrophages.

Immunometabolism, which examines the contribution of diverse metabolic pathways to the development, fate, and behavior of immune cells, has become an increasingly burgeoning research field in recent years.[20,21] Metabolic pathways are differentially regulated in M1 and M2 macrophages, and this is associated with their varying roles in the immune response. OXPHOS is associated with anti-inflammatory macrophages, whereas enhanced glycolysis has been associated with proinflammatory macrophages.[21] Exposing innate immune cells to an initial insult induces a long-term immune response due to metabolic and epigenetic alterations which encompass an emerging new concept called trained immunity.[41,42] Innate immune memory is currently regarded as a conserved defensive mechanism of monocytes, macrophages, and natural killer cells because this trained memory usually confers these cells enhanced responsiveness to future infections and pathogens.[41,43] These reprogramming processes of macrophages often occurred during their maturation. In our investigation, we showed GDF15 to be capable of reprogramming macrophages during their maturation. Such trained immune preference in macrophages imprinted by GDF15 is featured by reduced inflammation. These findings, along with our observations in vivo, in which the adoptive transfer of GDF15-preprogrammed macrophages alleviates liver injury and fibrosis, support future studies in which manipulation of metabolism in macrophages via GDF15 may provide a novel anti-inflammatory and antifibrogenic approach in the liver. In line with this, previous work showed the efficacy of the adoptive transfer of anti-

inflammatory macrophage to effectively reduce liver fibrosis in mice,[37] and more recently, macrophage therapy has been established as clinically safe supporting the use of these promising approaches to treat chronic liver disease.[44]

This study had some limitations. One question raised in our studies is what the source of GDF15 during pathophysiological processes could be. Critically, the tissue-specific site(s) of GDF15 production remain largely unknown. *Gdf15* mRNA is induced in the liver and adipose tissue in rodent models of obesity but not in skeletal muscle, heart, or kidney. Human data addressing this question are limited.[45,46] With regard to the liver, transcriptomic profiling and immunohistochemistry of samples from patients with moderate nonalcoholic fatty liver disease and advanced NASH, both of which strongly associate with obesity, demonstrated increased expression of *Gdf15* in hepatocytes and epithelial and immune cells of the liver from NASH samples.[47] Collectively, these data suggest that in rodents, liver or adipose tissue cell types may contribute to changes in circulating GDF15, whereas in humans, multiple cell types within the liver may be the primary source. Although our data clearly showed the importance of GDF15 in the pathogenesis of liver fibrosis, the identity of the cells producing GDF15 still awaits the availability of mice with cell type–specific conditional KO of GDF15. Additionally, we have clearly demonstrated that the effect of GDF15 is exerted through affecting macrophages; however, the exact receptor(s) that mediates the effects of GDF15 on macrophages remains to be determined. Determining the identity of the functional GDF15 receptor in the periphery, including in diverse immune cell types, is a clear priority. Several studies have already confirmed that GFRAL is restricted to AP and NTS neurons.[24] However, it is undeniable that cells elsewhere can respond to GDF15 despite the apparent lack of GFRAL expression. Interestingly, GDF15 modulation of integrin activation in neutrophils is mediated by GDF15 binding to the TGF-β receptor I/II complex,[48] suggesting that this receptor might also be the GDF15 receptor in other immune cells. Moreover, a more recent study demonstrated that CD48 can bind GDF15 in T cells.[49] Thus, critical evaluation and validation of candidate GDF15 receptors used by diverse lymphoid and myeloid cells will be important in advancing our understanding of the immunoregulatory actions of GDF15.

In summary, our results provide novel mechanistic insights into the role of GDF15 in regulating liver inflammation and warrant future research to define the potential of metabolic regulation of macrophages, via modulating GDF15, as a therapeutic approach to treat liver fibrosis.

Materials and Methods

Human Samples

An HCC progression tissue array (DP087Lv01) was purchased from Bioaitech (Xi'an, China).

Gdf15 *KO Mice*

Gdf15 KO mice are constructed by CRISPR/Cas-mediated genome engineering. The single guide RNA was designed and synthesized to target the exons 1–2 of the *Gdf15* gene (NM_011819; GemPharmatech, Nanjing, China). Cas9 and guide RNA are then coinjected into fertilized eggs for KO mouse production. The genotype is analyzed by PCR and sequencing. Mice were backcrossed to the C57BL/6 background for up to 8 generations for the studies described here. In general, both male ($Gdf15^{-/-}$) and female ($Gdf15^{-/-}$) *Gdf15* KO mice appeared healthy at birth and remained viable into adulthood. Unless otherwise stated, 6- to 8-week-old age- and sex-matched littermate mice were used in all experiments.

Murine Models

All animal experiments were approved by the Animal Ethics Committee of Anhui Medical University (Hefei, China) and carried out by the National Institutes of Health Guide for the Care and Use of Laboratory Animals. Male C57BL/6J WT mice at 6–8 weeks of age were obtained from the Animal Experiment Center of Anhui Medical University and housed in a specific pathogen–free animal facility. *Gdf15* KO mice (strain no. T011862) were purchased from GemPharmatech.

For toxic liver fibrosis, 6- to 8-week-old male WT and *Gdf15* KO mice were given intraperitoneal injections of CCl_4 (1.0 mL/kg body weight, dissolved in corn oil at a ratio of 1:9) (Aladdin, Shanghai, China) or vehicle (corn oil) twice a week for 4 or 6 weeks (n = 5 per group). The mice were sacrificed 2 days after the final CCl_4 injection. Some mice received repeated intraperitoneal injections of 200 μL liposomal clodronate (5 mg/mL) or liposomal vehicle as described.[36]

For the DDC diet, 8-week-old male WT and *Gdf15* KO mice were fed a diet supplemented with 0.1% DDC (Sigma-Aldrich, St. Louis, MO) for 5 weeks (n = 5 per group). Control mice received a standard mouse diet.

In the in vivo GDF15 treatment experiment, rmGDF15 (R&D Systems, Minneapolis, MN) was dissolved in 4 mM HCL and mixed with corn oil. Six- to 8-week-old male WT mice were injected with 100 ng/g per mouse of rmGDF15 or vehicle (corn oil) twice a week after each CCl_4 (1.0 mL/kg body weight, twice a week) injection from the second week to the fourth week (n = 5 per group).

Mouse AAV8 Construction and Injection

The AAV8 delivery system that overexpresses the mGDF15 gene in mouse livers was constructed by HanBio Biotechnology (Shanghai, China). The empty associated adenovirus (AAV8-null) served as a control. Titers of the vector genome were measured by quantitative qRT-PCR with vector-specific primers. The 6- to 8-week-old male WT mice were injected with 100 μL of virus containing 2×10^{11} AAV8 vector genomes via the tail vein for 2 weeks and then induced by CCl_4 (1.0 mL/kg body weight, twice a week) for another 4 weeks (n = 5 per group).

Quantitative Real-Time PCR

Total RNA was extracted from tissue samples or cells with TRIzol reagent (Invitrogen, Waltham, MA) followed by isopropyl alcohol precipitation. RNA concentration and quality were evaluated using Nano-drop system and was

then reverse-transcribed into complementary DNA by commercially available kit (Vazyme, Nanjing, China). SYBR green–based qRT-PCR kits (Vazyme) were used to perform mRNA quantification. Gene expressions were normalized to β-actin expression. Primer sequences are listed in Table 1.

Table 1. Primers Used to Amplify Target Gene Expressions for Quantitative Polymerase Chain Reaction

Gene	Primers (5′-3′)
Mouse Actb	Forward: TGGCTCCTAGCACCATGAAG Reverse: CGCAGCTCAGTAACAGTCCG
Mouse Acta2	Forward: GTTCAGTGGTGCCTCTGTCA Reverse: ACTGGGACGACATGGAAAAG
Mouse Col1a1	Forward: TAGGCCATTGTGTATGCAGC Reverse: ACATGTTCAGCTTTGTGGACC
Mouse Col1a2	Forward: AAGGGTGCTACTGGACTCCC Reverse: TTGTTACCGGATTCTCCTTTGG
Mouse Pdgfr	Forward: CCGTGGTCCCACATTCCTTG Reverse: GCACAGGGTCCACGTAGATG
Mouse Gdf15	Forward: AGCCGAGAGGACTCGAACTC Reverse: CTAGTGATGTCCCAGGGGCG
Mouse Nos2	Forward: TCCTGGACATTACGACCCCT Reverse: CTCTGAGGGCTGACACAAGG
Mouse IL-1β	Forward: GAAATGCCACCTTTTGACAGTG Reverse: TGGATGCTCTCATCAGGACAG
Mouse Tnf-α	Forward: CCAGACCCTCACACTCAGATCATC Reverse: GCGTAGACAAGGTACAACCCATCG
Mouse Sdhc	Forward: CAGGCCGGAACTCAAGATGG Reverse: TCCCAAAGGAGCAGCATTTC
Human ACTB	Forward: CATGTACGTTGCTATCCAGGC Reverse: CTCCTTAATGTCACGCACGAT
Mouse IL-6	Forward: AGACTTCCATCCAGTTGCCTT Reverse: TTCTCATTTCCACGATTTCCC
Mouse Arg1	Forward: CTCCAAGCCAAAGTCCTTAGAG Reverse: AGGAGCTGTCATTAGGGACATC
Mouse TGF-β	Forward: CGCCATCTATGAGAAAACCAA Reverse: GAGTTCCACATGTTGCTCCA
Mouse Ym1	Forward: CAGGTCTGGCAATTCTTCTGAA Reverse: GTCTTGCTCATGTGTGTAAGTGA
Mouse CD206	Forward: CTCTGTTCAGCTATTGGACGC Reverse: CGGAATTTCTGGGATTCAGCTTC
Mouse Ndufa7	Forward: AATATGGCGTCCGCTACTCG Reverse: TTGGACAGCTTGTGACTGGG
Mouse Uqcr11	Forward: CGGGGTGACCCTGAGTATTG Reverse: GATGTAAGGCACCCAGTCCA
Mouse Atp5j2	Forward: ACACCAGGACTTCAAGATGGC Reverse: ATACCGGTCATACCCTCTCC
Mouse Cox7c	Forward: TGGTACGGCCATTTCTTCCG Reverse: CACGGTCATCATAGCCAGCA
Human ACTA2	Forward: AAAAGACAGCTACGTGGGTGA Reverse: GCCATGTTCTATCGGGTACTTC
Human COL1A1	Forward: GTGCGATGACGTGATCTGTGA Reverse: CGGTGGTTTCTTGGTCGGT

Enzyme-Linked Immunosorbent Assay

IL-1β, IL-6, and TNF-α levels in mouse serum from the indicated treatment group were measured using the enzyme-linked immunosorbent assay (ELISA) development kits (R&D Systems) according to the manufacturer's instructions. Supernatants were stored at –80°C until used for ELISA. A450 value was used to measure the protein levels. The experiment was performed in triplicate at a minimum.

Mouse BMDM Isolation

Mouse BMDMs were prepared as previously described.[50,51] Briefly, bone marrow cells were flushed from tibias and femurs of 6- to 8-week-old male WT mice. Red blood cells were removed by Red Blood Cell Lysis Buffer. After washed, the cell suspension was passed a 40-μm cell strainer and plated in a 6-well plate at a density of 2×10^6 with 50 ng/mL macrophage colony-stimulating factor (ProteinTech, Rosemont, IL) in high-glucose Dulbecco's modified Eagle's medium (DMEM) with 10% fetal bovine serum (FBS), 100 U/mL of penicillin, and 100 mg/mL of streptomycin for 7 days. Fresh differentiation medium was added on day 4. To evaluate the role of GDF15 in macrophage polarizations, GDF15 (100 ng/mL) was added on days 1, 3, and 5. These cells were left untreated (as a control) or were treated with LPS (100 ng/mL; Sigma-Aldrich) + IFN-γ (20 ng/mL; ProteinTech) or IL-4 (20 ng/mL; ProteinTech) or recombinant GDF15 protein for 24 hours. The cells were collected for qRT-PCR.

Liver Macrophages Isolation

Liver macrophages were isolated from mice by portal perfusion using prewarmed solution containing 0.05% collagenase type IV dissolved in $Ca2^+$/$Mg2^+$ Hank's Balanced Salt Solution, filtered through a 40-μm nylon strainer (Falcon, Mexico City, Mexico) and were then subjected to 40 *g* centrifugation without brake. To enrich liver macrophages, nonparenchymal cells were suspended in Hank's Balanced Salt Solution and layered onto a 2-layer 25%–50% Percoll gradient (Sigma-Aldrich) in a 50-mL conical centrifuge tube and centrifuged at 1800 *g* at 4°C for 15 minutes. Liver macrophages in the middle layer were collected and allowed to attach to cell culture plates in supplemented DMEM with 10% FBS for 20 minutes at 37°C. Nonadherent cells were removed by replacing the culture medium. The purity of macrophages in the adherent cells was determined by immunofluorescent staining with anti-F4/80.

Liver Histological and Immunohistochemistry Staining

H&E staining and Sirius red or Masson's trichrome staining were performed to assess hepatic morphology and liver fibrosis, respectively. Liver specimens were fixed in 4% paraformaldehyde solution, embedded in paraffin, and cut into 5-μm sections. Next, the specimens were deparaffinized, hydrated, and stained by using commercial H&E staining kit and Sirius red or Masson's trichrome staining kit according to the manufacturer's instructions. Hepatic fibrosis was graded according to Ishak scoring system: grade 0, no fibrosis; grade 1, fibrous expansion of some portal areas with or without short fibrous septa; grade 2, fibrous expansion of most portal areas, with or without short fibrous septa; grade 3, fibrous expansion of most

portal areas with occasional portal-to-portal bridging; grade 4, fibrous expansion of portal areas with marked bridging (portal to portal as well as portal to central); grade 5, marked bridging (portal to portal and/or portal to central) with occasional nodules (incomplete cirrhosis); and grade 6, cirrhosis, probable or definite. The cumulative histologic scores could have ranged from 0 (entirely normal) to 6 (severe disease with cirrhosis).

For immunohistochemistry staining, 5-μm formalin-fixed, paraffin-embedded sections were deparaffinized, hydrated at first, and then incubated in 3% hydrogen peroxide solution for 5 minutes to block endogenous peroxidase. Antigen retrieval was performed by heating the sections in 0.01 M sodium citrate buffer solution (pH 6.0) for 10 minutes at 95°C. Liver sections were permeabilized with 0.5% Triton X-100 for 20 minutes and blocked in 5% bovine serum albumin solution for 40 minutes in room temperature, followed by incubating with primary antibody against GDF15 (1:300; Abcam, Cambridge, United Kingdom), F4/80 (1:200; Cell Signaling Technology, Danvers, MA), α-SMA (1:300; Abcam), MPO (1:300; Abcam), and P65 (1:300; Abcam) at 4°C overnight. Sections were incubated with secondary antibodies (ZSGB-Bio, Beijing, China) and DAB, followed by brief counterstaining with H&E staining, and mounted with neutral gum.

Immunofluorescence Staining

For immunofluorescence staining, briefly, for tissue samples, formaldehyde-fixed, paraffin-embedded slides were subjected to dewaxing, hydration, and antigen retrieval, followed by blocking and antibody incubation. For in vitro experiments, cells were seeded on coverslips and were fixed with 3% paraformaldehyde, permeated with 0.1% Triton X-100 followed by 10% bovine serum albumin blockage. Primary antibodies were diluted as suggested, added onto slides and were incubated at 4°C overnight in a moist chamber. Then slides were washed with phosphate-buffered saline and incubated with 488/594/horseradish peroxidase–conjugated secondary antibodies. For immunofluorescence staining, slides were further incubated with DAPI (Invitrogen) and mounted in immunofluorescence mounting medium (Servicebio, Woburn, MA).

Extracellular Flux Analysis

Extracellular flux analysis of macrophages was prepared as previously described.[50] XF base medium (Seahorse, La Verne, CA; 102353-100) was warmed to 37°C and supplied with 10 mM glucose, 2 mM glutamine, and 2 mM pyruvate. Adjust medium pH to 7.4 using 1 N NaOH and filter sterilize medium with a 0.22-μM filter. Macrophages were seeded in Seahorse XF24 microplate (Agilent, Santa Clara, CA) and cultured with the prepared XF medium. The cell culture microplate was placed in a 37°C non-CO_2 incubator for 1 hour prior to the assay. Load oligomycin into port A, FCCP to port B and rotenone/antimycin to port C of the hydrated sensor cartridge. The OCR and ECAR of macrophages were then determined after sequentially administration of the following reagents (final concentration): 1.0 μM oligomycin (Selleck Chemicals, Houston, TX; S1478), 0.75 μM FCCP (Sigma-Aldrich; C2920), and 100 nM rotenone (Sigma-Aldrich; R8875) + 1.0 μM antimycin (BioVision, Exton, PA; 2247-50) using the extracellular flux analyzer.

Enzymatic Assay for Mitochondrial Complex

Macrophage mitochondria were isolated using kit from Solarbio Science & Technology Co, Ltd (Beijing, China). The isolated mitochondria were subjected to test the activities of mitochondrial complexes using commercial kits from Solarbio Science & Technology Co, Ltd.

Flow Cytometry

Intrahepatic leukocytes were isolated as described.[35,52] Multicolor staining was conducted using combinations of the following monoclonal antibodies: CD45, CD11b, Ly6C, Ly6G, F4/80, CD3, CD4, CD8, and B220 (eBioscience [San Diego, CA] or BioLegend [San Diego, CA]). Data were acquired from a FACS Caliber system (BD, Franklin Lakes, NJ) and analyzed using FlowJo (TreeStar, Ashland, OR).

LX-2 Culture and Treatment

LX-2, a human immortalized HSC line, was cultured in DMEM supplemented with 10% FBS and 1% penicillin/streptomycin at 37°C in a humidified atmosphere containing 5% CO_2. LX-2 cells were seeded in 6-well plates, and cells were stimulated by indicated CM from BMDMs in the absence or presence of TGF-β1 for 24 hours. The cells were collected for quantitative PCR.

Serum Biochemistry

Serum levels of ALT and AST were measured by using commercial alanine aminotransferase assay kit and aspartate aminotransferase assay kit (#C009-2-1 and #C010-2-1; Nanjing Jiancheng Bioengineering Institute, Nanjing, China) according to the manufacturer's instructions.

Measurement of Hepatic Hydroxyproline Content

Fresh mouse liver samples were used to quantify the hepatic hydroxyproline content. Measurements were done by using commercial hydroxyproline assay kit (#A030-2-1; Nanjing Jiancheng Bioengineering Institute) according to the manufacturer's instruction.

Terminal Deoxynucleotidyl Transferase–Mediated dUTP Nick-End Labeling

TUNEL staining of liver tissue was performed using a TUNEL Apoptosis Detection Kit (Alexa Fluor 488; Yeasen Biotech Co, Ltd, Shanghai, China) according to the manufacturer's protocol.

Statistical Analysis

Values in this study were expressed as mean ± SEM. Statistical analysis was performed using GraphPad Prism 9 software (GraphPad Software, San Diego, CA). Differences between 2 groups were analyzed using the 2-tailed, unpaired Student t test. Differences between more than 2

groups were analyzed by using 1-way analysis of variance, followed by Dunnett's multiple comparisons test. $P < .05$ was considered statistically significant.

References

1. Koyama Y, Brenner DA. Liver inflammation and fibrosis. J Clin Invest 2017;127:55–64.
2. Wick G, Grundtman C, Mayerl C, et al. The immunology of fibrosis. Annu Rev Immunol 2013;31:107–135.
3. Asrani SK, Devarbhavi H, Eaton J, et al. Burden of liver diseases in the world. J Hepatol 2019;70:151–171.
4. Phadke I, Dwivedi A, Taylor N. Turning the tide: From fibrosis to regeneration following anti-fibrogenic cell vaccination. Cell Stem Cell 2022;29:1421–1423.
5. Hernandez-Gea V, Friedman SL. Pathogenesis of liver fibrosis. Annu Rev Pathol 2011;6:425–456.
6. Wick G, Backovic A, Rabensteiner E, et al. The immunology of fibrosis: innate and adaptive responses. Trends Immunol 2010;31:110–119.
7. Pellicoro A, Ramachandran P, Iredale JP, et al. Liver fibrosis and repair: immune regulation of wound healing in a solid organ. Nat Rev Immunol 2014;14:181–194.
8. Wynn TA, Vannella KM. Macrophages in tissue repair, regeneration, and fibrosis. Immunity 2016;44:450–462.
9. Guillot A, Tacke F. Liver macrophages: old dogmas and new insights. Hepatol Commun 2019;3:730–743.
10. Kisseleva T, Brenner D. Molecular and cellular mechanisms of liver fibrosis and its regression. Nat Rev Gastroenterol Hepatol 2021;18:151–166.
11. Tacke F. Targeting hepatic macrophages to treat liver diseases. J Hepatol 2017;66:1300–1312.
12. Baeck C, Wei X, Bartneck M, et al. Pharmacological inhibition of the chemokine C-C motif chemokine ligand 2 (monocyte chemoattractant protein 1) accelerates liver fibrosis regression by suppressing Ly-6C(+) macrophage infiltration in mice. Hepatology 2014;59:1060–1072.
13. Kazankov K, Jørgensen SMD, Thomsen KL, et al. The role of macrophages in nonalcoholic fatty liver disease and nonalcoholic steatohepatitis. Nat Rev Gastroenterol Hepatol 2019;16:145–159.
14. Murray PJ. Macrophage polarization. Annu Rev Physiol 2017;79:541–566.
15. Mossanen JC, Krenkel O, Ergen C, et al. Chemokine (C-C motif) receptor 2-positive monocytes aggravate the early phase of acetaminophen-induced acute liver injury. Hepatology 2016;64:1667–1682.
16. Ramachandran P, Pellicoro A, Vernon MA, et al. Differential Ly-6C expression identifies the recruited macrophage phenotype, which orchestrates the regression of murine liver fibrosis. Proc Natl Acad Sci U S A 2012;109:E3186–E3195.
17. Bartneck M, Fech V, Ehling J, et al. Histidine-rich glycoprotein promotes macrophage activation and inflammation in chronic liver disease. Hepatology 2016;63:1310–1324.
18. Beattie L, Sawtell A, Mann J, et al. Bone marrow-derived and resident liver macrophages display unique transcriptomic signatures but similar biological functions. J Hepatol 2016;65:758–768.
19. Ganeshan K, Chawla A. Metabolic regulation of immune responses. Annu Rev Immunol 2014;32:609–634.
20. O'Neill LA, Kishton RJ, Rathmell J. A guide to immunometabolism for immunologists. Nat Rev Immunol 2016;16:553–565.
21. O'Neill LA, Pearce EJ. Immunometabolism governs dendritic cell and macrophage function. J Exp Med 2016;213:15–23.
22. Bootcov MR, Bauskin AR, Valenzuela SM, et al. MIC-1, a novel macrophage inhibitory cytokine, is a divergent member of the TGF-beta superfamily. Proc Natl Acad Sci U S A 1997;94:11514–11519.
23. Lemmelä S, Wigmore EM, Benner C, et al. Integrated analyses of growth differentiation factor-15 concentration and cardiometabolic diseases in humans. Elife 2022;11:e76272.
24. Luan HH, Wang A, Hilliard BK, et al. GDF15 is an inflammation-induced central mediator of tissue tolerance. Cell 2019;178:1231–1244.e11.
25. Aguilar-Recarte D, Barroso E, Palomer X, et al. Knocking on GDF15's door for the treatment of type 2 diabetes mellitus. Trends Endocrinol Metab 2022;33:741–754.
26. Zhang Y, Zhao X, Dong X, et al. Activity-balanced GLP-1/GDF15 dual agonist reduces body weight and metabolic disorder in mice and nonhuman primates. Cell Metab 2023;35:287–298.e4.
27. Reyes J, Yap GS. Emerging roles of growth differentiation factor 15 in immunoregulation and pathogenesis. J Immunol 2023;210:5–11.
28. Coll AP, Chen M, Taskar P, et al. GDF15 mediates the effects of metformin on body weight and energy balance. Nature 2020;578:444–448.
29. Day EA, Ford RJ, Smith BK, et al. Metformin-induced increases in GDF15 are important for suppressing appetite and promoting weight loss. Nat Metab 2019;1:1202–1208.
30. Laurens C, Parmar A, Murphy E, et al. Growth and differentiation factor 15 is secreted by skeletal muscle during exercise and promotes lipolysis in humans. JCI Insight 2020;5:e131870.
31. Abulizi P, Loganathan N, Zhao D, et al. Growth differentiation factor-15 deficiency augments inflammatory response and exacerbates septic heart and renal injury induced by lipopolysaccharide. Sci Rep 2017;7:1037.
32. Wang D, Day EA, Townsend LK, et al. GDF15: emerging biology and therapeutic applications for obesity and cardiometabolic disease. Nat Rev Endocrinol 2021;17:592–607.
33. Zhang J, He L, Wang Z, et al. Decreasing GDF15 promotes inflammatory signals and neutrophil infiltration in psoriasis models. J Invest Dermatol 2023;143:419–430.e8.
34. Xi Y, LaCanna R, Ma HY, et al. A WISP1 antibody inhibits MRTF signaling to prevent the progression of established liver fibrosis. Cell Metab 2022;34:1377–1393.e18.
35. She S, Wu X, Zheng D, et al. PSMP/MSMP promotes hepatic fibrosis through CCR2 and represents a novel therapeutic target. J Hepatol 2020;72:506–518.
36. Pradere JP, Kluwe J, De Minicis S, et al. Hepatic macrophages but not dendritic cells contribute to liver

fibrosis by promoting the survival of activated hepatic stellate cells in mice. Hepatology 2013;58:1461–1473.
37. Thomas JA, Pope C, Wojtacha D, et al. Macrophage therapy for murine liver fibrosis recruits host effector cells improving fibrosis, regeneration, and function. Hepatology 2011;53:2003–2015.
38. Duffield JS, Forbes SJ, Constandinou CM, et al. Selective depletion of macrophages reveals distinct, opposing roles during liver injury and repair. J Clin Invest 2005;115:56–65.
39. Jung SB, Choi MJ, Ryu D, et al. Reduced oxidative capacity in macrophages results in systemic insulin resistance. Nat Commun 2018;9:1551.
40. Lee SE, Kang SG, Choi MJ, et al. Growth differentiation factor 15 mediates systemic glucose regulatory action of T-helper type 2 cytokines. Diabetes 2017;66:2774–2788.
41. Netea MG, Joosten LA, Latz E, et al. Trained immunity: a program of innate immune memory in health and disease. Science 2016;352:aaf1098.
42. Sohrabi Y, Godfrey R, Findeisen HM. Altered cellular metabolism drives trained immunity. Trends Endocrinol Metab 2018;29:602–605.
43. Netea MG, van der Meer JW. Trained immunity: an ancient way of remembering. Cell Host Microbe 2017;21:297–300.
44. Moroni F, Dwyer BJ, Graham C, et al. Safety profile of autologous macrophage therapy for liver cirrhosis. Nat Med 2019;25:1560–1565.
45. Patel S, Alvarez-Guaita A, Melvin A, et al. GDF15 provides an endocrine signal of nutritional stress in mice and humans. Cell Metab 2019;29:707–718.e8.
46. Xiong Y, Walker K, Min X, et al. Long-acting MIC-1/GDF15 molecules to treat obesity: evidence from mice to monkeys. Sci Transl Med 2017;9:eaan8732.
47. Govaere O, Cockell S, Tiniakos D, et al. Transcriptomic profiling across the nonalcoholic fatty liver disease spectrum reveals gene signatures for steatohepatitis and fibrosis. Sci Transl Med 2020;12:eaba4448.
48. Artz A, Butz S, Vestweber D. GDF-15 inhibits integrin activation and mouse neutrophil recruitment through the ALK-5/TGF-βRII heterodimer. Blood 2016;128:529–541.
49. Wang Z, He L, Li W, et al. GDF15 induces immunosuppression via CD48 on regulatory T cells in hepatocellular carcinoma. J Immunother Cancer 2021;9:e002787.
50. Du L, Lin L, Li Q, et al. IGF-2 preprograms maturing macrophages to acquire oxidative phosphorylation-dependent anti-inflammatory properties. Cell Metab 2019;29:1363–1375.e8.
51. Li X, Su X, Liu R, et al. HDAC inhibition potentiates anti-tumor activity of macrophages and enhances anti-PD-L1-mediated tumor suppression. Oncogene 2021;40:1836–1850.
52. Li S, Zhou B, Xue M, et al. Macrophage-specific FGF12 promotes liver fibrosis progression in mice. Hepatology 2023;77:816–833.

Received April 4, 2023. Accepted July 19, 2023.

Correspondence
Address correspondence to: Hanren Dai, PhD, Department of Oncology, the First Affiliated Hospital of Anhui Medical University, 218 Jixi Road, Hefei 230022, China. e-mail: daihanren0321@126.com; or Hua Wang, MD, PhD, Department of Oncology, the First Affiliated Hospital of Anhui Medical University, 218 Jixi Road, Hefei 230022, China. e-mail: wanghua@ahmu.edu.cn.

CRediT Authorship Contributions
Xiaolei Li (Conceptualization: Equal; Funding acquisition: Lead; Investigation: Lead; Methodology: Lead; Supervision: Lead; Writing – original draft: Lead)
Qian Huai (Data curation: Equal; Methodology: Equal; Software: Equal)
Cheng Zhu (Investigation: Equal; Methodology: Equal)
Xu Zhang (Formal analysis: Supporting; Methodology: Supporting; Software: Supporting)
Wentao Xu (Resources: Supporting; Software: Supporting; Validation: Supporting)
Hanren Dai (Funding acquisition: Equal; Project administration: Equal; Supervision: Equal; Writing – original draft: Equal)
Hua Wang, prof (Conceptualization: Equal; Investigation: Equal; Project administration: Lead; Supervision: Equal; Writing – review & editing: Equal)

Conflicts of Interest
The authors disclose no conflicts.

Funding
This study was supported by grants from the National Natural Science Foundation of China (grant nos. 82270622 and 82270641) and the Postdoctoral Science Foundation of China (grant no. 2021M690184).